The Thesis Committee for Meredith Moss Evans
certifies that this is the approved version of the following thesis:

Evaluation of petroleum hydrocarbon weathering on coastal Louisiana
beaches and salt marshes following the *Deepwater Horizon* oil spill using
ramped pyrolysis – gas chromatography – mass spectrometry

APPROVED BY
SUPERVISING COMMITTEE:

Supervisor:

Zhanfei Liu

Amber K. Hardison

Brad E. Rosenheim

Evaluation of petroleum hydrocarbon weathering on coastal Louisiana beaches and salt marshes following the *Deepwater Horizon* oil spill using ramped pyrolysis – gas chromatography – mass spectrometry

by

Meredith Moss Evans, B.S.

Thesis

Presented to the Faculty of the Graduate School of

The University of Texas at Austin

in Partial Fulfillment

of the Requirements

for the Degree of

Master of Science in Marine Science

The University of Texas at Austin

May 2016

Dedication

Firstly, I dedicate this to my parents, Jim and Tamara Evans, for using all their resources to selflessly prioritize my aspirations and for being my first, and best, friends. I thank my dad for always laughing at me when I need to stop taking myself so seriously, and my mom for answering the phone at 5am and bringing humor to any situation. I thank my papa and nana, Noble and Catharine Moss, for helping my parents support my dreams and papa, for being the best example that you choose any career and if you love it, the money will come. I wholeheartedly thank Matthew Seeley for being my partner in everything and the greatest thing I found in my Master's. Finally, I thank Donald Shimoda, for the reoccurring reminder that if you argue your limitations, sure enough, they're yours.

Acknowledgements

Abstract

Evaluation of petroleum hydrocarbon weathering on coastal Louisiana beaches and salt marshes following the *Deepwater Horizon* oil spill using ramped pyrolysis – gas chromatography – mass spectrometry

Meredith Evans, M.S. Marine Sci.
The University of Texas at Austin, 2016

Supervisor: Zhanfei Liu

In spring of 2010, the *Deepwater Horizon* oil spill polluted hundreds of miles of coastline in the Gulf of Mexico. A combination of human-mediated and natural weathering processes then altered the chemical composition (i.e. toxicity) of this spilled crude oil over time and space. One of the most important, yet challenging, aspects of oil spill science is to quantify these chemical changes in natural environments. In this study we evaluate the chemical transformation of petroleum hydrocarbons from the *Deepwater Horizon* spill on a coastal Louisiana beach and salt marsh from 2010-2012.

Using gas chromatographic analysis, we quantify the depletion of *n*-alkanes, polycyclic aromatic hydrocarbons (PAHs), alkylated PAHs and hopanes relative to source oil to evaluate weathering trends across spatial and temporal differences. We report overall depletion of low molecular weight (LMW) *n*-alkanes and PAHs in all locations with time. The magnitude of depletion at any given time, however, depends on

the sampling location, whereby the sites with the highest wave energy have the highest percentage of compound depletion. Oiled sediment from an enclosed bay shows highest retention of high molecular weight (HMW) PAHs, which may have been contributed from sources other than the *Deepwater Horizon* spill. This provides information regarding where petroleum hydrocarbons are likely to persist in coastal environments, which can be used to inform policy makers and responders for future petroleum pollution.

In addition, we confirm these results with the novel application of ramped pyrolysis – gas chromatography – mass spectrometry (Py-GC-MS). We show that bulk flow Py-GC-MS can quantify overall weathering degree of oil samples, and that thermal slicing Py-GC-MS can quantify specific petroleum hydrocarbons as well as qualify changes in non-GC amenable petroleum hydrocarbons with weathering. Our data suggests an increase in HMW (i.e. resin and asphaltene) petroleum fractions and oxygenated products with weathering. This analysis not only elucidates weathering trends with current samples, but also illustrates the analytical capacity of this method for future petroleum hydrocarbon investigations.

Keywords: petroleum hydrocarbon, weathering, wave energy, Deepwater Horizon, oil spill, salt marsh, ramped pyrolysis, analysis technique, thermal slicing, oxygenated hydrocarbon, asphaltene, resin

Table of Contents

List of Tables

List of Figures

Introduction

On April 20, 2010 an explosion of the *Deepwater Horizon* oil rig initiated the uncapping of the deep sea Macondo wellhead. In the 87 days the wellhead was uncapped, approximately 5 million barrels of crude oil were spilled and 1,773 km of shoreline were oiled, making it the largest accidental oil spill in history.[1-3] Estimates suggest that ~17% was directly recovered from the wellhead, 13% naturally dispersed, 23% evaporated or dissolved, 16% was chemically dispersed, 5% was burned, 3% was skimmed and 10% remains on the sea floor.[4,5] Of these processes, only direct recovery and skimming completely remove petroleum hydrocarbons from the marine environment. Therefore, around 80% of Macondo well oil remained in marine ecosystems following this spill.

The fate of this remaining oil is determined by weathering processes, including biodegradation, photooxidation, evaporation, dissolution and emulsification. The first two processes can manipulate the chemical structure of the petroleum hydrocarbon, while the latter three either separate or coalesce petroleum hydrocarbons.[6,7] Understanding these weathering processes is crucial to predicting petroleum hydrocarbon persistence and toxicity, but can be largely variable depending on a variety of factors such as the spill site hydrography, weather, and type of oil.

To better predict hydrocarbon persistence as a function of weathering, research has largely focused on evaluating the concentrations of petroleum hydrocarbons over time and space following the *Deepwater Horizon* spill.[2,3,7-14] These studies focus on two of the four main petroleum hydrocarbon classes: saturates and aromatics. Saturates include *n*-alkanes, alkenes, cycloalkanes, etc. and are largely non-toxic. Aromatics

include polycyclic aromatic hydrocarbons (PAHs) and their alkylated homologues, which pose toxicity threats to a variety of species.[15] In comparison to source oil, these studies report rapid loss of low molecular weight (LMW) compounds, particularly of *n*-alkanes $<C_{20}$ and single ring PAHs. With time, concentrations of more complex petroleum hydrocarbons have been reported to further deplete, with the exception of some high molecular weight (HMW) PAHs recorded in coastal salt marsh sediment.[8]

Traditionally, these depletions are reported relative to recalcitrant internal biomarker, $17\alpha(H),21\beta(H)$-hopane. This molecule is resistant to weathering; therefore, it is common to measure analyte concentration relative to $17\alpha(H),21\beta(H)$-hopane concentration, in order to adjust to the degree of original oiling.[16] It is also common to use similar molecules, hopanes and steranes, to determine the source of the petroleum hydrocarbons in a sample because the ratio of these compounds is dependent on source oil.[17] There has been some work suggesting that some biomarkers degraded following the *Deepwater Horizon* spill, but a few, particularly hopanes and norhopanes, are resistant and can be used for source identification.[18]

The analytical instrumentation used to analyze these biomarkers, aromatics and saturates consists primarily of gas chromatography – mass spectrometry (GC-MS) and gas chromatograph – flame ionization detection (GC-FID). There are limitations to these techniques, however. For example, the other two hydrocarbon classes, resins and asphaltenes, have been largely ignored in response to the *Deepwater Horizon* because the analytical techniques are unable to analyze their complex hydrocarbon structures due to their extremely low volatility.[19,20] In addition, compounds oxidized by photooxidation and

biodegradation cannot be measured using traditional methods.[21,22] There have been many advances in analytical instrumentation, particularly Fourier transform ion cyclotron resonance mass spectrometry, which can identify HMW and oxidized hydrocarbons, but cannot reliably quantify their content.

In order for response to future oil spills to continue to improve, there is need for advancement in these fields. First of all, current evaluation of saturated and aromatic hydrocarbons largely focuses on one or two ecosystem over time. There is little comparison of hydrocarbon retention between ecosystems over time. This type of comparison can expand knowledge about how different ecosystems are likely to respond to hydrocarbon pollution, allowing for better prioritization of remediation efforts. In addition, expansion should focus on quantification of resins, asphaltenes and oxygenated hydrocarbons. These hydrocarbons are complex and likely to persist in the environment, but little is known about their exact characteristics and thus, toxicity threats.

In this research, we seek to use traditional analysis and novel method application to expand these areas of interest. In Chapter 1, we utilize traditional analysis techniques to highlight petroleum weathering patterns in coastal ecosystems over time. We find that weathering is dependent on wave energy and that multiple sources, outside of the *Deepwater Horizon* spill may have been contributing to this pattern. In Chapter 2, we innovatively employ ramped pyrolysis - gas chromatography - mass spectrometry to analyze environmental oiled samples. We show the efficiency of this technique to not only quantify traditionally measured petroleum hydrocarbons, but also compare the

weathering degree of non-traditionally evaluated hydrocarbons, which highlights the

increased complexity of petroleum with advanced environmental weathering.

Chapter 1. Petroleum Hydrocarbon Persistence following the *Deepwater Horizon* Oil Spill as a Function of Shoreline Energy

ABSTRACT

In summer of 2010, the *Deepwater Horizon* oil spill polluted hundreds of miles of coastline in the Gulf of Mexico. A combination of human-mediated and natural weathering processes then altered the chemical composition (i.e. toxicity) of this spilled crude oil over time and space. One of the most important aspects of oil spill science is to quantify these chemical changes in natural environments. In this study we evaluate the chemical transformation of petroleum hydrocarbons from the *Deepwater Horizon* spill on a coastal Louisiana beach and salt marsh from 2010-2012. Using gas chromatographic analysis, we quantify the depletion of *n*-alkanes, PAHs, alkylated PAHs and hopanes relative to source oil to evaluate weathering trends across spatial and temporal differences. We report overall depletion of LMW *n*-alkanes and PAHs in all locations with time. The magnitude of depletion at any given time, however, depends on the sampling location, whereby the sites with the highest wave energy have the highest percentage of compound depletion. Oiled sediment from an enclosed bay shows highest retention of HMW PAHs, which may be from sources other than the *Deepwater Horizon* spill. This provides information regarding where oil is likely to persist in coastal environments, which can be used to inform policy makers and responders for future petroleum pollution.

Keywords petroleum hydrocarbon, weathering, wave energy, *Deepwater Horizon*, oil spill, salt marsh

INTRODUCTION

Each year, millions of barrels of petroleum seep into the Gulf of Mexico, with varying sources contributing to this leakage - natural seeps, tanker spillages and drilling accidents.[23–25] The *Deepwater Horizon* oil spill in April of 2010 was the largest accidental oil spill ever recorded, releasing ~5 million barrels of oil into the Gulf of Mexico.[3,26] Although this was catastrophic for ocean-based industry and marine ecosystems alike, scientists have utilized this spill as a case study for petroleum hydrocarbon degradation and transformation in marine environments. The overall goal of these studies has been to better understand and respond to future oceanic petroleum pollution.[27]

Accomplishing this goal, however, is difficult because every oil spill is unique – the hydrocarbon composition of the crude, the weather/currents at the time of the spill, and the hydrographic features of polluted areas all vary. In addition, processes that weather, i.e. change the chemical composition of, crude oil change dramatically across space and time.[28] These processes have been extensively studied in field and lab cases since the *Deepwater Horizon* spill and include evaporation,[7,10,19] dissolution,[2,3] emulsification,[29] biodegradation,[11,30–33] chemical transformation[20–22,34] and sedimentation.[5,7] It is nearly impossible to summarize these variable processes across locations to gain a holistic view of the fate of petroleum hydrocarbons; rather, researchers must focus on how combinations of particular conditions drive hydrocarbon degradation and thus, toxicity.

Shoreline energy and geography is one such component of oil spill restoration research. In 1974, Rashid evaluated the degradation of Bunker C oil after a spill in Nova

Scotia and reported advanced dispersion and biodegradation in high energy environments.[35] Following the *Exxon Valdez* spill in Alaska, researchers documented entrainment of oil in protected shorelines,[36,37] and later researchers summarized how variable combinations of low shoreline energy and protected coastal geography have led to multi-decadal persistence of petroleum following various oil spills.[38]

In 2014, Pendergraft and Rosenheim analyzed how the hydrography of a barrier island and coastal salt marsh in Louisiana affected the degradation of petroleum from the *Deepwater Horizon*.[39] Using ramped pyrolysis ^{14}C analysis they proved persistence of petroleum hydrocarbons up to 2.5 years following the spill, but demonstrated that the thermochemical stability of these hydrocarbons changed. In highly oiled samples collected soon after the spill, the hydrocarbon signature consisted of relatively labile organic material; as time passed, this shifted to a more recalcitrant hydrocarbon signature. Interestingly, these patterns were found across locations, not just over time, whereby weathering (i.e. depletion of labile petroleum hydrocarbons) was most advanced in high energy sites and least advanced in a sheltered bay.

In this study, we evaluate the compound specific composition of the samples collected by Pendergraft and Rosenheim, 2014.[39] The ramped pyrolysis method these authors used elegantly detailed the evolution of organic material based on thermal stability, but did not give compound-specific insight. This is important in order to (a) confirm the persistence or degradation of labile petroleum hydrocarbons at different geographic locations and (b) quantify persistence of toxic petroleum components, particularly polycyclic aromatic hydrocarbons (PAHs), which pose threats to humans and

marine species.[40,41] We use gas chromatographic analysis to quantify PAHs, their alkylated homologues (alkylated PAHs), *n*-alkanes, and hopanes present in oiled samples and compare these concentrations to crude oil released from the Macondo wellhead during the *Deepwater Horizon* spill. We observe enhanced retention of petroleum hydrocarbons, particularly high molecular weight (HMW) PAHs and alkylated PAHs in the low energy environments, which we speculate could be from sources additional to the *Deepwater Horizon*. We also confirm that amongst samples collected at the same time, weathering is most enhanced at the high energy beach location, followed by the low energy beach location and finally, the protected salt marsh. This is useful for predicting locations that will be most affected in future oil spills and prioritizing remediation efforts.

METHODS

Sample Collection

Oiled sediment, tar and oil sheen samples were collected from Grand Isle and Bay Jimmy, LA (29.258°N 89.958°W and 29.477°N 89.894°W, respectively) in conjunction with Pendergraft and Rosenheim, 2014.[39] Briefly, all samples were collected within 881 days following uncapping of the Macondo wellhead (20 April 2010) that initiated the *Deepwater Horizon* spill. Oil sheen sample was collected floating at Grand Isle, Louisiana after 46 days. Oiled sediment was collected at Grand Isle after 88, 337 and 678 days from either a high energy location, exposed to direct wave impact from the Gulf of Mexico, or a low energy site, located on the lagoonal side of the tidal inlet at the NE tip of Grand Isle and sheltered from wave energy (Figure 1). Sediment samples obtained at 88 d were collected from the surface sand layer, which was visibly oiled. Samples

collected at 337 d and 678 d were collected from a buried, visibly oiled layer, approximately 1 meter deep (Figure 2). Sediment from Bay Jimmy was collected after 694 d via sediment core in the intertidal zone; oiled sediment was sampled from the visibly oiled layer, ~1 cm deep. Tar samples were collected after 337 d along the coast of Bay Jimmy and 881 d at Grand Isle, LA. Samples were placed in precombusted glassware and immediately stored at -4°C under nitrogen gas. Prior to chemical analysis, samples were freeze dried for 24 h. Macondo well crude oil ("MW crude oil") was obtained from the National Institute for Standards and Technology (NIST) and used for comparison.

Chemical Analysis

Each sample was analyzed for n-alkanes (C_{10}-C_{40}), 16 priority EPA PAHs, alkylated and other PAHs, hopanes and steranes (Table 1 for the list of compounds with abbreviations) following the procedure by Liu et al., 2012.[7] Briefly, ~1 g of sample was weighed, spiked with hexadecane-d_{34}, fluorine-d_{10} and benzo(e)pyrene-d_{12}, and extracted with dichloromethane for 24 h using Soxhlet extraction. Following procedures in Wang et al. 2004,[42] samples were fractionated in a column packed with 3 g activated silica gel and topped with 3-5 g anhydrous sodium sulfate. Following column conditioning with 20 mL hexanes, saturated hydrocarbons were eluted and collected with 12 ml of hexanes, followed by aromatic hydrocarbon elution and collection in 15 mL of hexanes and benzenes (1:1). These fractions were concentrated with Rotovap to a final volume of 100 μL. Total GC-detectable saturated n-alkanes were analyzed using GC-MS (Shimadzu GCMS-OP2010). Total PAHs and alkylated PAHs were analyzed with GC-FID

(Shimadzu GC-2014). Selective Ion Mode was used for calculation (ion list in Table A.1). Final concentrations were determined in $\mu g_{analyte} \ g_{sample}^{-1}$.

Quality Control and Quality Assurance

A five-point standard curve was used for quantification. Hexadecane-d_{34}, fluorine-d_{10} and benzo(*e*)pyrene-d_{12} spikes were used to adjust for analytical percent recovery. All solvents were chromatographic grade and purchased from either Fisher Scientific or Sigma-Aldrich. Laboratory techniques for crude oil and weathered petroleum analysis were confirmed to be equivalent with other marine organic chemistry laboratories by participation in an interlaboratory calibration as reported during the Gulf of Mexico Research Initiative conference in February of 2010.

Data Analysis

We compared biomarker ratios of MW crude oil to all samples collected using recalcitrant MW hopane ratios, 17α(H)-22,29,30-trisnorhopane:17α(H),21β(H)-hopane and 17α(H),21β(H)-30-norhopane:17α(H),21β(H)-hopane.[18] Samples that deviated ±0.06 from either MW ratio value were designated as having a primary source other than MW oil, and were removed from the remainder of data analysis.[43]

The concentration of measured *n*-alkanes, PAHs, alkylated PAHs and hopanes (Table A.2) for each sample (C_S) was normalized to the concentration of 17α(H),21β(H)-hopane[16] (H_S), hereby referred to as C_{30}-hopane ratio. These ratios were used to calculate the compound percent depletion relative to MW crude using equation 1.1, in which the compound concentration in MW oil (C_O) was also normalized to C_{30}-hopane concentration in MW oil (H_O). This percent depletion approach has been used by

10

previous studies to evaluate weathering of petroleum hydrocarbons because it estimates

the relative change in concentration compared to source oil, while also adjusting for the

magnitude of original pollution at a particular location.[10,43]

$$(1.1) \quad \% \text{ depletion} = \left[\left[\frac{C_O}{H_O} - \frac{C_S}{H_S} \right] \middle/ \frac{C_O}{H_O} \right] \times 100$$

Percent depletions were statistically compared between sediments collected at

different locations within the same time period (i.e. 88 d high and low energy sediment,

678 d high and low energy sediment, 678 d low energy and 694 d bay sediment). Non-

parametric Wilcox signed-rank test (non-parametric) was used in R console to compare

the difference between pairs compound depletion measurements, where H_0=percent

depletions are not significantly different amongst compounds and H_A=percent depletions

are significantly greater in the higher energy environment.

RESULTS

Biomarker analysis confirmed most samples sourced from MW crude. The ratios

of 17α (H)-22,29,30-trisnorhopane:C_{30}-hopane and 17α(H),21β(H)-30-norhopane:C_{30}-

hopane for MW oil were approximately 0.23 and 0.56, respectively. Samples used for

this study fell into the range of 0.19-0.25 and 0.51-0.62, respectively (Figure 1.3). Of all

samples collected, one oiled sediment sample and three tar samples were determined not

from MW source and excluded from further analysis.

The majority of compounds showed significant depletion compared to crude oil,

with rapid depletion of *n*-alkanes and low molecular weight PAHs (Table 1.1). For

example, Nap was >99% depleted in all samples and total n-alkanes were >80% depleted

within 337 d. Some compounds, however, showed a negative percent depletion, i.e. an

increase in concentration relative to Macondo crude oil, primarily in PAHs (BkF, IndP,

DA and GHI) and alkylated PAHs (Flua1, Flua3, BeP, and Pry). Moreover, the 694 d bay

sediment sample had the highest number of compounds increase in concentration (33

compounds) and the highest magnitude of compound increase, with a percent depletion

of total 16 priority EPA PAHs at -20.08% and other PAHs at -348.96%, compared to a

range of 74.84 - 97.88% for total 16 priority EPA PAHs and -11.27 - 68.11% for total

other PAHs in all other samples.

We also compared the percent depletions based on geographic location, including

all compounds for sediment collected at low and high energy sites after 88 d (Figure

1.4A). For alkanes, the low energy site shows a higher percent depletion up to C_{32}, after

which the pattern switches and low energy sites show lower percent depletions. For

PAHs and alkylated PAHs, the high energy site shows lower percent depletion across all

compounds except perylene and benzo(e)pyrene. Excluding these outliers, Wilcox

signed-rank test indicates that the high energy site had significantly greater depletion than

the low energy site (p=0.04944). Also compared were the percent depletions for high and

low energy sediment collected after 678 d on Grand Isle and sediment collected after 694

d in Bay Jimmy (Figure 1.4B). The percent depletion, considering all compounds, for 678

d high energy site was significantly higher than low energy site (Wilcox signed-rank test

p=0.005766) and the 678 d low energy sediment had significantly higher depletion than

the 694 bay sediment (Wilcox signed-rank test p=0.00222). Exceptions to this trend

include IndP, DA and GHI, in which the 678 d low energy sediment has the lowest percent depletion followed by 694 d bay and then 678 d high energy sediment, as well as anthracene and 3-methylchrysene, in which the depletion is lowest in the high energy environment. Overall, however, there is significantly higher depletion at high energy sites for measured compounds.

DISCUSSION

Enhanced Compound Concentrations

In response to the *Deepwater Horizon* spill, many studies have evaluated petroleum weathering along oiled coastlines.[7,8,10,12–14,22,31,43,44] Although many of these employed the same percent depletion calculations, only one has reported amplified relative chemical concentrations.[8] Therefore, we first address the detection of enhanced compound concentrations in our samples. There are two primary hypotheses for how this compound enrichment could occur: (1) C_{30}-hopane was degraded at a faster rate than the compounds of interest, thereby overestimating the relative compound retention, or (2) there are external sources of enhanced compounds, in addition to MW crude oil.

To address the first hypothesis, we must consider the robustness of our C_{30}-hopane inert compound. The use of this compound is motivated by the need to qualify how much compound is in a sample (C_S) relative to how much that sample was originally oiled (H_S). Studies using MW crude have observed degradation of traditional biomarker compounds (i.e. hopanes, steranes and triaromatic steroids), whereby triaromatic steroids were the fastest degraded,[10] followed by homohopanes.[18] These studies, however, did not find C_{30}-hopane to be significantly degraded. A comprehensive study by Stout et al.

$(2016)^{10}$ reported several absolute concentrations within samples (C_S) higher than that of crude oil (C_O), but with C_{30}-hopane normalization only reported depletion relative to crude oil. Turner et al. 2014 also reported enhanced concentrations of HMW PAHs following the *Deepwater Horizon* spill in a coastal salt marsh, similar to our study. We, however, not only observe higher C_S than C_O in samples (Table A.2), but also higher C_S/H_S than C_O/H_O ratios, causing the negative percent depletion values.

To determine if this might be caused by a C_{30}-hopane depletion, the most enriched sample (694 d bay sediment) was chosen to calculate the minimum C_{30}-hopane concentration required to adjust all the percent depletions >0. This would require C_{30}-hopane value of 59,930ng g^{-1}, which is ~95 times the concentration we actually detected (629.1ng g^{-1}). Similarly, C_{30}-hopane in the second most enriched sample (678 d low energy sediment) would have to reach 17,600ng g^{-1}, ~86 times the actual C_{30}-hopane detected (204.2ng g^{-1}). Estimates of homohopane degradation by Aeppli et al. 2014[18] reached a maximum of 55% relative to MW oil, thus we conclude >85% depletion of C_{30}-hopane in our samples unlikely. In addition, the C_{30}-hopane concentration in crude oil is only 56000 ng g^{-1}, meaning our bay sediment sample would have to be more concentrated than the MW oil. These estimates imply it unlikely that C_{30}-hopane degradation is the major cause of the enhanced concentration.

An alternative explanation for the enhanced concentration is input from external sources. To test this hypothesis, we focus on the most enhanced compounds: PAHs with >4 benzene rings and alkylated PAHs. Known sources of PAHs to the coastal environment include, in order of lowest to highest contribution, wastewater runoff,

industrial effluent, atmospheric deposition of combusted fossil fuels or coals and combustion of biomass.[45–48] Although it is difficult to pinpoint these sources, specific PAH ratios are often employed to determine if PAHs are petrogenic (crude oil) or pyrogenic (organic material combustion) in origin.[45,49] Here, we use ratios BaA/[BaA+Chr] and IndP/[IndP+GHI] because these are the HMW PAHs of interest, their relative ratios are less likely to be altered by petroleum weathering processes.[45,49,50] Crude oil is the most distinct sample, with completely petrogenic origin, whereas all other samples show some potential pyrogenic or mixed source signature (Figure 1.5). The locations that have mixed source or slightly pyrogenic signatures (i.e. all samples excluding 678 d low energy and 694 d bay sediment) may be attributable to controlled landscape burning prior to or in response to the *Deepwater Horizon* spill. The most pyrogenic sediment sample was collected in Bay Jimmy (694 bay sediment), near the Mississippi River. The river carries a wide variety of effluent from agricultural or industrial centers that may be enriched in 3-6 ring PAHs from fossil fuel burning, which could be leaching into sediments from the river and/or groundwater, causing the high pyrogenic signature.[51] Most importantly, the relative pyrogenic signature is highest in samples with a high number and magnitude of PAH concentration increase, which supports the hypothesis that PAH enrichment is caused by externals sources such as river input, atmospheric deposition and precipitation.

We also consider non-pyrogenic, external hydrocarbon sources, such as marine biota. For example, perylene enrichment could be explained by anthropogenic input or diatom degradation, which causes the relatively ubiquitous presence of perylene in anoxic

and oxic marine sediments.[52] We observe minor enrichment of alkanes, C_{26} and C_{27}, particularly C_{27}, in the 88 d high energy sediment and C_{14}-C_{16}, particularly C_{15}, in the 694 d bay sediment. This increase is not likely attributable to weathering of MW oil, as evaporation would deplete LMW compounds and biodegradation would deplete mid-MW compounds.[7,11] However, addition of marine and aquatic plankton may account for this increase, as many species have a dominant C_{14}-C_{27} alkane signature, and of those alkanes odd number chains dominate.[53,54]

These hydrocarbon sources help explain the percent retention relative to MW crude; however, the absolute concentration should also be considered. For example, benzo[k]fluoranthene in the 694 d bay sediment sample has a depletion of -9427.19%, which corresponds to ~94 times the C_{30}-hopane ratio in MW crude. The absolute concentration (without C_{30}-hopane normalization) in the sample is 0.24μg mg^{-1}, which is only ~20% the actual concentration in MW crude oil (1.15μg mg^{-1}). This is often the case, where the enhanced concentrations are driven by the C_{30}-hopane normalization, but the actual concentration is relatively equivalent or even lower than MW crude. Therefore, these retained compounds are not necessarily at toxic concentrations.

Furthermore, this data would have been greatly enhanced by comparison to baseline data showing the concentration of these pollutants in sediments pre-spill. A study by Turner et al. 2014, used similar analysis methods to quantify petroleum hydrocarbons in a marsh before and after the *Deepwater Horizon* spill and found significant concentrations of some PAHs, including Nap, Nap1, BaP, DahA and GHI before the spill and persistence of these compounds after the spill. This corroborates not

only our conclusion that external sources might have been polluting our sediments

(particularly the marsh) before the *Deepwater Horizon* spill, but also corroborates that

some of the compounds we find to be most enriched have shown similar enrichment

previously.

Geographic Weathering Trends

Amongst sediment samples collected at or around the same time, there is a clear

pattern of decreased compound depletion in lower energy, more geographically isolated

environments. Figure 1.4A compares sediment collected after 88 d in high and low

energy locations on Grand Isle, LA. Oiling at this time was tidally controlled, so Grand

Isle sites were oiled within 6 hours of each other. The HMW *n*-alkanes, PAHs and

alkylated PAHs show higher depletion in the high energy sites than the low energy sites,

suggesting advanced weathering in high energy environments. This is likely due to

advanced dispersion from wave action on the beach, which enhances dissolution and

increases surface area for biodegradation.[35,38] The LMW *n*-alkanes, conversely, are more

highly depleted in the low energy environment. This site is further inland and would have

been oiled slightly after the high energy site, so this may be a result of advanced

evaporation, which is one of the dominant processes of LMW hydrocarbon weathering

and extremely time dependent.[28] The only other compounds that deviate from this pattern

are Pry and BeP. As previously discussed, Pry is ubiquitously found in marine sediments

and has a variety of sources; therefore, we cannot easily specify what causes the

deviation here. Arulazhagan et al. (2014) studied biodegradation of BeP by

Achromobacter sp. and *Marinobacter* sp. and found that enhanced BeP degradation

occurred when Phe was available as co-substrate.[55] Phe in this site was already absent, potentially leading to the enhanced retention of BeP.

In samples collected between 678 d and 694 d following the *Deepwater Horizon* spill, we also observe decreased weathering at low energy sites (Figure 1.4B). The lowest energy site (Bay Jimmy) showed more enrichment compared to MW crude, while other sites showed more depletion. The most advanced depletion is at the high energy Grand Isle site, which, once again, is likely attributed to high wave energy effectively dispersing oil and promoting bacterial activity. Rarely, this pattern reverses and the bay site has the highest depletion, followed by Grand Isle sites. This is observed most predominantly in 3Chr and Acy. Chrysenes have shown to have atypical degradation patterns in previous research, such that molecules with higher degrees of methylation are preferentially degraded by photooxidation.[6,10,43] This does not specifically explain the reverse pattern observed here, but does suggest that abnormal weathering patterns for Chr3 are not uncommon. We also cannot explain the deviation for Acy, except to speculate that this may be a result of photooxidation reaction interferences[56] and highlight the variability of Acy concentrations in oil-sand aggregates from the *Deepwater Horizon*.[14]

Overall, the predominating pattern amongst all samples is highest degradation in high energy environments. Could this pattern, however, be a function of PAH addition from external sources in low energy environments, and not just a function of MW crude weathering? We have already shown that the majority of samples showed biomarker signature from the *Deepwater Horizon,* but also had mixed or non-petrogenic signatures. To determine whether crude oil weathering is causing our degradation patterns, we

employ weathering proxies. The number of rings in PAHs should increase with weathering; that is, PAHs with 2 rings tend to be preferentially removed by weathering.[28,57] Our samples show that 2 ring PAHs are most relatively abundant in Crude oil, followed by 694 bay sediment and 678 low energy sediment. This suggests that less weathering has occurred in low energy sediments relative to high energy sediments, because high energy sites are more depleted in LMW PAHs (Figure A.1).

Another weathering proxy we utilized is the ratio of alkylated PAHs to non-alkylated PAHs. This ratio is commonly employed because weathering will preferentially deplete non-alkylated PAHs, leading to a high alkylated:non-alkylated ratio.[28,57] The relative alkylation is higher in the high energy Grand Isle sediments than the low energy sediments (Figure 1.6), confirming increased weathering at the high energy sites. The bay sediment sample, however, shows the highest alkylation, suggesting that it had weathered the most. This may be a result of alkylated PAHs from external sources, mentioned previously; theoretically, these would be highly weathered (and thus, mostly alkylated) by the time they reached Bay Jimmy, supporting this high alkylation pattern. Overall, it difficult to definitively determine the weathering degree of *Deepwater Horizon* oil in these sediment samples. We can, however, conclude that the bay has entrained more PAHs than sediments from Grand Isle (Table A.2) and that compound concentration patterns are likely a mixed result of MW oil weathering and addition of other hydrocarbon sources.

Further support for weathering patterns described here derives from the work of Pendergraft and Rosenheim, 2014. We used the same samples as these authors, but with

19

different analytical methods, to describe weathering patterns.[39] They utilized ramped pyrolysis radiocarbon (^{14}C) analysis, and found that all samples had a strong isotopic signature of petrocarbon, confirming that all our samples were oiled by the *Deepwater Horizon* spill and nearly devoid of radiocarbon. This does not contradict our source data presented in Figure 1.5, but rather, confirms that a mixture of MW oil and other pyrogenic sources contributed to hydrocarbon content. They also found that the thermochemical stability of the samples changed, whereby older, higher energy environment samples showed higher organic stability relative to crude oil. This increase in thermochemical stability suggests a decrease in labile petroleum hydrocarbons, or an increase in weathering.[58] Our results also demonstrate that GC detectable (i.e. labile) hydrocarbons decrease with increased shoreline energy, confirming their thermochemical stability results. Note that the persisting radiocarbon signature they find in highly weathered samples is likely due to petroleum hydrocarbons outside of our analytical window, such as asphaltene and resin components. In conjunction with this study, we conclude that (1) all samples were oiled by the *Deepwater Horizon* spill and (2) weathering degree varies between high energy and low energy environments, as confirmed by compound quantification and ramped pyrolysis analysis.

Sediment composition is also an important clue to describe these weathering patterns. Locations on Grand Isle, LA are sandy beaches with medium grain size, which highlights their high energy nature compared to the very fine silt and clay particles present at Bay Jimmy (Figure 1.1). Previous studies have evaluated petroleum persistence based on sediment type, and reported that oil is most likely to persist in fine, organic

sediment.[1,8,15,35,36,59–61] Turner et al. (2014) suggest that persistence of petroleum

hydrocarbons in marsh sediments is partially a function of this low energy sediment type,

which has higher sportive capacity and lower dissolved oxygen for biodegradation.[8]

Silliman et al. (2012) highlight how variable subsidence and erosion actually magnified

petroleum pollution issues on the seaward edge of marshes in Barataria Bay following the

Deepwater Horizon spill, supporting the effect fine grain size sediment movement has on

petroleum hydrocarbon persistence.[62] Therefore, the weathering trends are not necessarily

a direct result of wave energy, but the effect wave energy has on the sediment

composition and thus, compound retention.

CONCLUSIONS

  We examine the weathering of petroleum hydrocarbons following the *Deepwater*

Horizon oil spill from a multi-factor data set that includes compound-specific changes

over time (881 d) and space, from a high energy shoreline, low energy barrier island and

protected coastal salt marsh. All samples described showed evidence of MW oiling and,

in most cases, we observe compound degradation relative to MW oil with time. Our

lowest energy site, a salt marsh within an enclosed bay, showed a high degree of relative

compound increase, primarily of HMW PAHs. This could be attributed to additional

sources other than the *Deepwater Horizon* spill such as combustion of gasoline, coal or

biomass, suggested by PAH ratios that indicate pyrogenic origin. Weathering proxies,

however, confirm high weathering in high energy locations and low weathering in low

energy locations, consistent with the work of Pendergraft and Rosenheim (2014).[39] This

emphasizes (1) the importance of physical advection of oiled water and sediments in

order to advance weathering processes such as evaporation, dissolution and biodegradation, (2) the effect of low energy sediment composition on the sorption and retention of complex petroleum hydrocarbons and (3) the contribution of external sources to hydrocarbon content in coastal Louisiana salt marshes. These data should help effectively inform responders that sheltered locations with minimal wave energy are likely to have long term ramifications following future oil spills, thus helping to prioritize remediation efforts.

CHAPTER 1 TABLES

Table 1.1 Percent depletion for each compound. All samples organized by energy type and labeled based on collection date on Grand Isle, with the exception of sample denoted with * which was collected in Bay Jimmy.

Compound Name & Abbreviation		Oil Sheen	Tar Balls		Low Energy Sediments			High Energy Sediments		
		46.0	337.0	881.0	88.0	678.0	694*	88.0	337.0	678.0
C_{10} alkane	C_{10}	100.0	100.0	100.0	100.0	100.0	100.0	100.0	100.0	100.0
C_{11} alkane	C_{11}	100.0	100.0	100.0	99.9	98.8	98.2	99.9	99.7	99.3
C_{12} alkane	C_{12}	99.5	99.6	98.9	99.8	97.8	90.4	99.9	95.7	96.9
C_{13} alkane	C_{13}	99.9	99.6	99.2	99.8	98.2	69.9	99.9	99.8	99.5
C_{14} alkane	C_{14}	99.8	99.6	99.1	99.8	95.5	-15.9	99.8	99.7	99.5
C_{15} alkane	C_{15}	98.9	99.6	98.9	99.7	93.0	-48.2	99.7	99.4	99.5
C_{16} alkane	C_{16}	95.5	99.3	98.4	99.3	92.6	-16.5	99.3	98.2	99.1
C_{17} alkane	C_{17}	86.9	98.7	97.8	98.9	94.9	44.3	95.2	96.5	98.8
C_{18} alkane	C_{18}	68.5	97.1	96.5	96.5	95.3	78.1	75.5	92.5	98.1
C_{19} alkane	C_{19}	49.5	87.1	95.4	87.0	97.3	93.2	53.5	86.6	98.5
C_{20} alkane	C_{20}	20.2	92.3	92.4	57.3	95.8	94.7	19.9	74.9	98.1
C_{21} alkane	C_{21}	20.6	96.1	93.8	41.0	96.5	95.2	20.6	81.4	98.2
C_{22} alkane	C_{22}	16.1	96.6	93.6	19.4	96.0	94.3	13.1	80.7	97.4
C_{23} alkane	C_{23}	13.6	96.4	92.7	12.6	95.7	91.6	5.0	81.9	97.3
C_{24} alkane	C_{24}	18.7	96.1	92.8	13.0	95.8	92.2	8.0	83.6	97.1
C_{25} alkane	C_{25}	26.2	87.2	92.3	16.5	96.2	87.9	4.8	84.7	97.4
C_{26} alkane	C_{26}	11.9	95.4	90.7	15.9	95.4	91.5	-1.7	85.2	97.2
C_{27} alkane	C_{27}	8.4	96.4	89.6	13.3	94.6	71.9	-4.7	87.9	96.1
C_{28} alkane	C_{28}	12.3	95.4	88.6	8.0	94.4	84.8	3.9	88.1	96.0
C_{29} alkane	C_{29}	13.1	94.3	86.5	10.6	92.7	36.9	4.6	88.8	95.6

Table 1.1 Continued

C_{30} alkane	C_{30}	17.5	91.1	83.3	20.4	92.9	81.0	8.4	86.8	95.5
C_{31} alkane	C_{31}	17.7	88.1	82.3	14.2	92.4	32.3	13.0	85.7	95.5
C_{32} alkane	C_{32}	24.8	79.7	76.1	22.1	91.5	80.3	21.7	82.9	95.9
C_{33} alkane	C_{33}	25.0	57.5	68.2	20.0	90.2	49.0	25.5	71.2	93.0
C_{34} alkane	C_{34}	34.3	45.8	60.2	28.8	90.6	82.6	38.1	64.3	95.0
C_{35} alkane	C_{35}	40.5	34.7	56.1	33.9	90.5	74.2	49.1	62.0	93.2
C_{36} alkane	C_{36}	50.5	43.3	57.0	35.3	87.8	80.8	52.1	70.9	92.1
C_{37} alkane	C_{37}	39.2	25.1	45.0	24.1	84.8	76.2	44.7	62.9	90.2
Σ[Alkanes]		19.3	86.6	85.7	16.9	94.2	80.8	11.2	81.9	96.2
Naphthalene	Nap	99.8	99.8	99.4	99.6	98.7	95.3	99.8	99.9	99.7
Acenaphthylene	Acy	100.0	100.0	100.0	100.0	100.0	100.0	100.0	100.0	83.8
Acenapthelene	Ace	93.4	100.0	100.0	85.5	23.3	-680.9	93.1	98.4	92.8
Fluorene	Fl	97.8	97.4	93.8	96.3	62.7	-266.6	98.3	98.5	96.5
Phenanthrene	Phe	93.9	97.2	93.4	96.6	75.8	-185.7	98.4	97.1	97.1
Anthracene	An	72.2	65.4	13.8	48.5	-64.3	-854.0	74.1	90.4	71.6
Fluoranthene	Flua	57.2	36.7	-45.5	27.0	-99.8	-305.1	63.8	79.3	34.6
Pyrene	Pyr	67.7	73.3	27.9	63.3	5.1	-109.5	81.9	82.6	63.4
Benz[a]anthracene	BaA	55.2	17.1	-95.6	3.6	-158.8	-263.5	46.3	83.5	36.9
Chrysene	Chr	77.2	63.2	45.7	62.5	40.6	42.5	80.8	86.2	73.4
Benzo[b]fluoranthene	BbF	37.1	22.7	-104.3	-35.7	-249.9	-260.1	24.0	59.3	-5.0
Benzo[k]fluoranthene	BkF	-838	-2204.4	-5592	-2402	-8521	-9428	-1562	-506	-1584
Benzo[a]pyrene	BaP	-2.8	-80.8	-337.8	-209.2	-810.2	-915.6	-120.2	49.5	-45.5
Indeno[1,2,3-cd]pyrene	IndP	-505	-1570	-3989	-2116	-7592	-6770	-1690	-292	-971
Dibenz[a,h]anthracene	DA	-25.9	-252.4	-805.3	-453.3	-2076.7	-1369.1	-435.6	11.1	-133.8
Benzo[ghi]perylene	GHI	-7.7	-121.1	-379.7	-174.5	-874.3	-807.0	-103.0	39.6	-58.6
Σ[16 priority EPA PAHs]		96.0	94.9	88.6	93.1	74.8	-20.1	95.8	97.9	95.2
2-methylnaphthalene	Nap2	98.4	93.0	82.6	96.7	77.3	-178.2	98.4	98.0	93.8

24

Table 1.1 Continued

2,6-dimethylnaphthalene	Nap2,6	76.4	12.3	-116.9	48.7	-1380.4	-16967	75.0	75.5	29.9
2,3,5-trimethylnaphthalenne	Nap2,3,5	99.0	99.5	98.6	99.0	53.5	-298.7	99.6	99.5	99.4
1-methylfluorene	Fl1	33.6	86.0	66.1	69.5	-551.4	-4440.9	86.1	69.7	37.1
Dibenzothiophene	Dbt	65.6	70.3	29.2	77.0	-81.0	-2016.6	87.9	82.9	18.0
3-methylphenanthrene	Phe3	-60.1	57.8	-3.8	47.0	-121.2	-1369.6	67.5	40.7	56.6
2-methylphenanthrene	Phe2	-116.9	51.1	-20.2	32.8	-171.0	-2043.9	57.1	16.8	57.6
2-methylanthracene	An2	27.9	-64.5	-327.3	-51.1	-527.6	-4357.5	25.9	52.7	-33.1
9-methylphenanthrene	Phe9	-77.3	65.0	13.7	53.4	-41.8	-683.9	64.6	39.9	66.1
1-methylphenanthrene	Phe1	-102.5	52.8	-13.6	29.7	-114.2	-1088.6	55.4	18.5	46.1
4,6-dimethyldibenzothiophene	Dbt4,6	76.5	96.5	91.5	93.7	77.0	49.9	96.0	92.4	81.4
1,7-dimethylphenanthrene	Phe1,7	67.5	92.8	81.7	83.9	67.9	50.3	91.6	81.8	91.7
3 and 1-methylfluoranthene	Flua1&3	-75.7	-47.5	-401.5	-100.0	-287.5	-472.9	23.7	-15.2	-143.9
Retene	Ret	56.9	43.5	-58.1	50.4	-12.2	-45.5	80.9	64.8	10.6
1-methylpyrene	Pyr1	69.8	78.8	27.5	70.3	41.2	20.1	87.7	81.2	59.4
4-methypyrene	Pyr4	64.7	71.8	-2.3	53.5	-18.6	-86.6	78.9	82.3	63.0
3-methylchrsene	Chr3	82.7	5.8	-39.7	81.9	66.6	61.9	92.1	35.7	-9.5
6-methylchrsene	Chr6	55.4	90.1	43.3	39.0	-10.6	-30.0	76.9	66.0	35.0
Benzo(e)pyrene	BeP	4.9	-25.3	-298.4	-35.7	-289.8	-334.2	-172.7	47.0	-24.2
Perylene	Pry	-609	-2278	-7440	-1310	-8984	-12746	-6945	-483	-1573
Σ[Alkylated & Other PAHs]		30.3	60.3	4.6	62.8	-11.3	-349.0	68.1	61.2	46.8
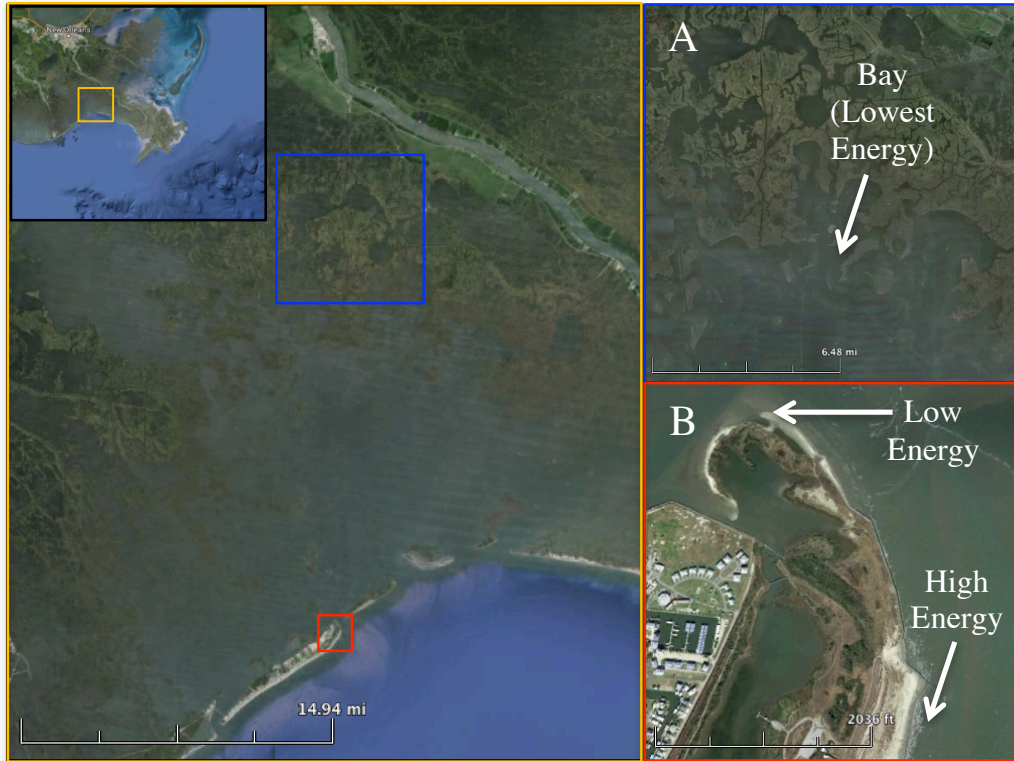
Figure 1.1 Sampling sties at Bay Jimmy within Barataria Bay, LA (A) and on Grand Isle, LA (B). Sites are labeled based on wave energy in 1A. The bay site in Figure 1B is considered to be the lowest energy site because barrier islands at the mouth of Barataria Bay protect it from direct wave energy. Within yellow outlined map, zoom of 1A is in blue square and 1B in blue square. Perspective of yellow outlined map is provided in black outlined map, which shows Mississippi River and New Orleans.
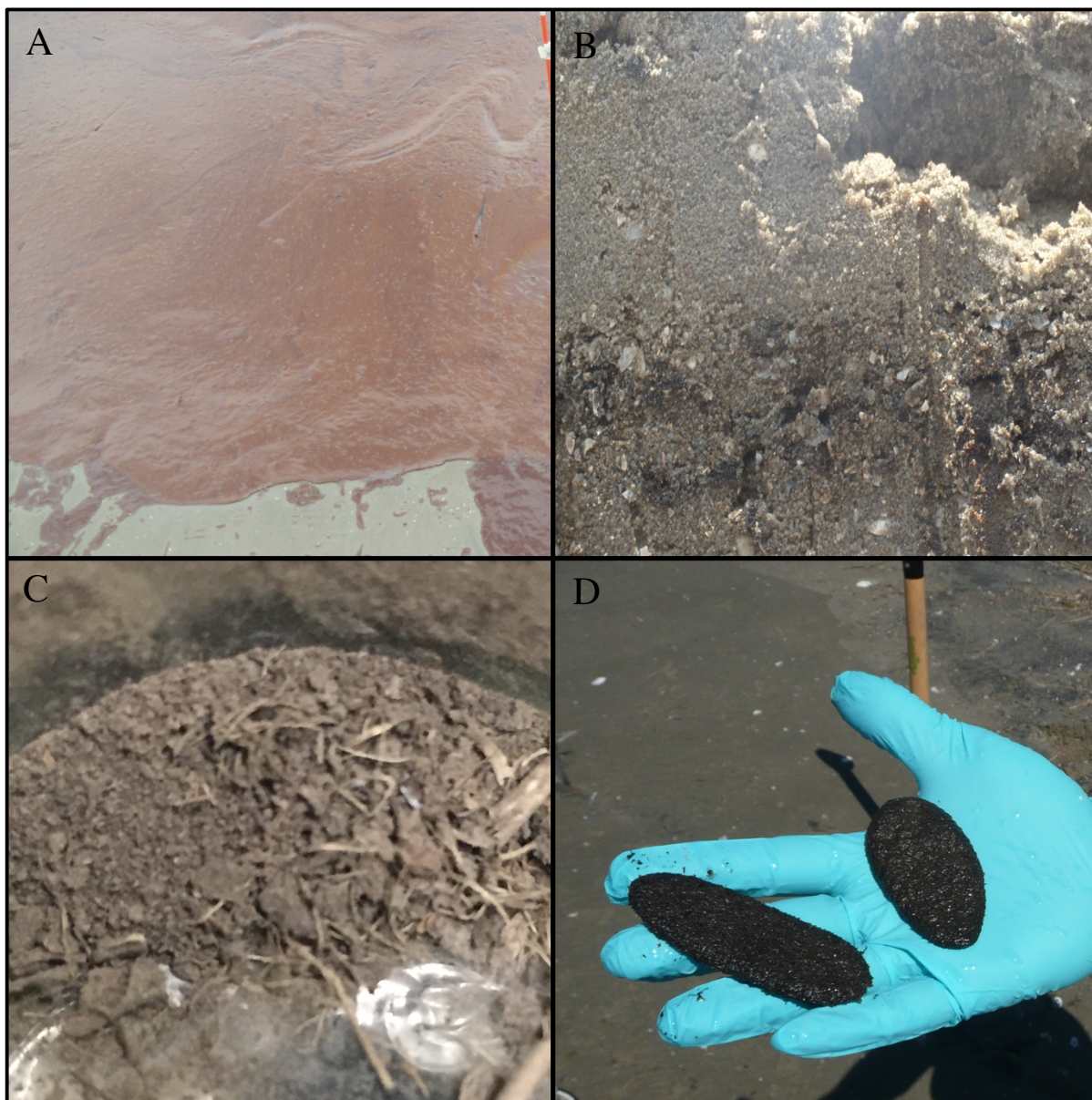
Figure 1.2. Images of some of the samples collected. A) Oil sheen collected after 46 d. B) Oiled sediment collected on Grand Isle after 678 d; sample was collected from the visibly oiled layer, ~1 m deep. (Samples collected on Grand Isle at 88 d were collected from the surface sediment layer, which was visibly oiled.) C) Dried sediment collected from Bay Jimmy. The sediment is visibly composed of fine particles and no sand. D) Tar collected from Grand Isle after 881 d.
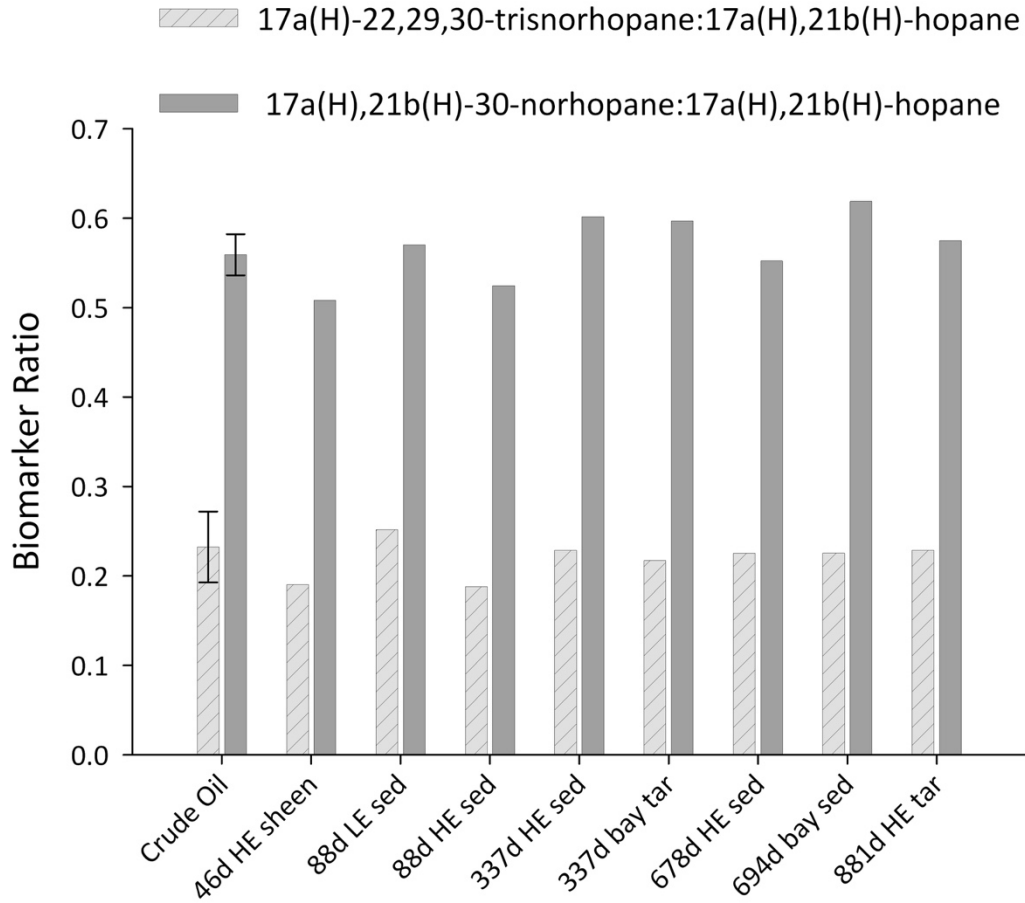
Figure 1.3. Biomarker ratios (17α(H)-22,29,30-trisnorhopane:17α,21β(H)-hopane and 17α(g)21β(H)-30-norhopane:17α(H),21β(H)-hopane) were used to confirm samples were oiled by MW oil. Samples labeled by collection date, site (high energy = HE, low energy = LE) and type (sed = sediment). Samples shown were all from MW oil. (Crude oil n=3.)
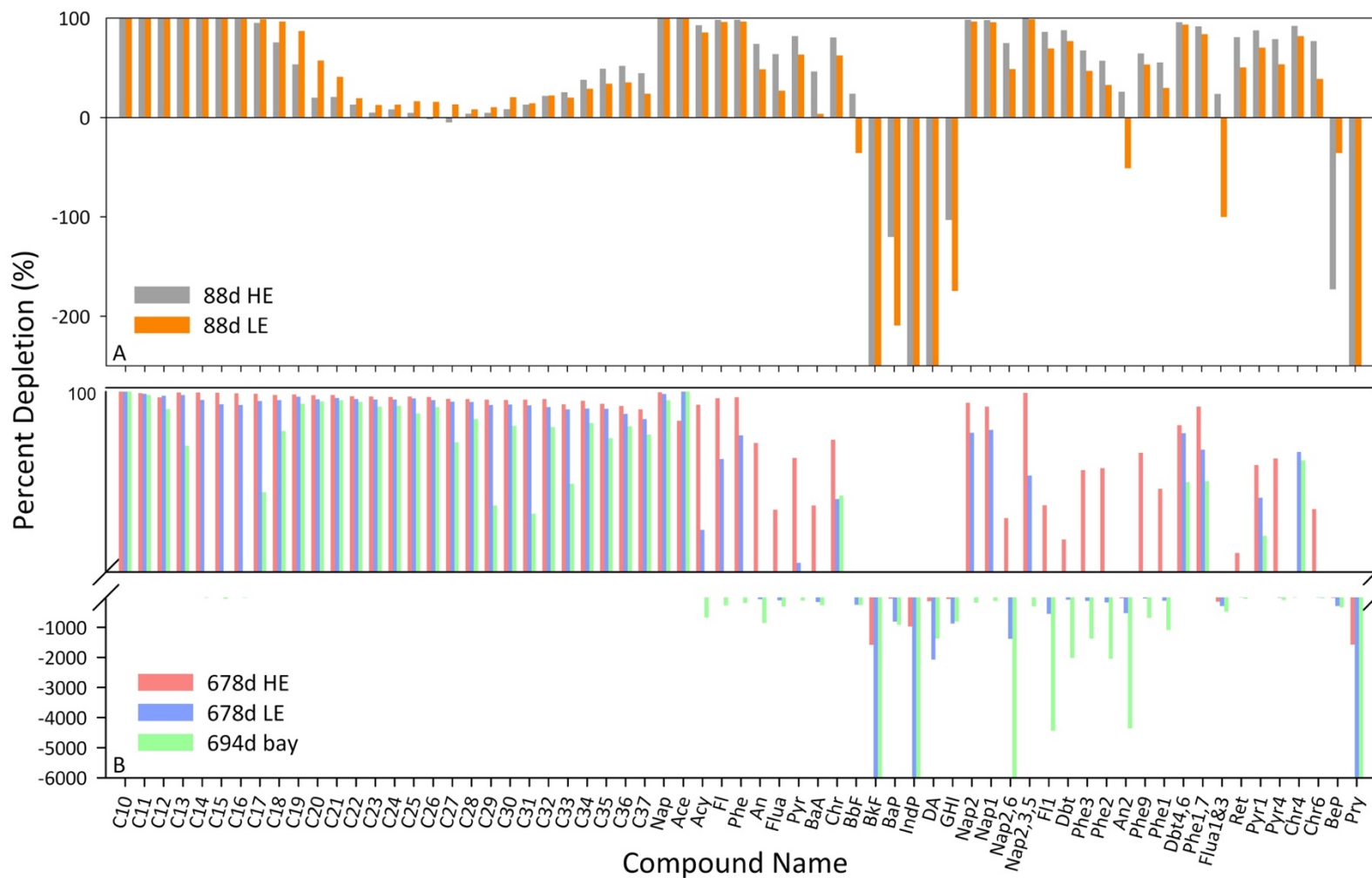
Figure 1.4. Compound percent depletion for 5 sites, with sediment samples collected (A) after 88 d at high and low energy Grand Isle sites, and (B) after 678 d high and low energy Grand Isle sites and after 694 d at Bay Jimmy, the lowest energy site. The overall pattern shows that among samples collected around the same time, percent depletion is highest at high energy locations. (Wilcox signed-rank test 88 d HE v. LE, p=0.04944; 678 d HE v. LE, p=0.005766; 678 d LE v. 694 d bay, p=0.00222.)

29
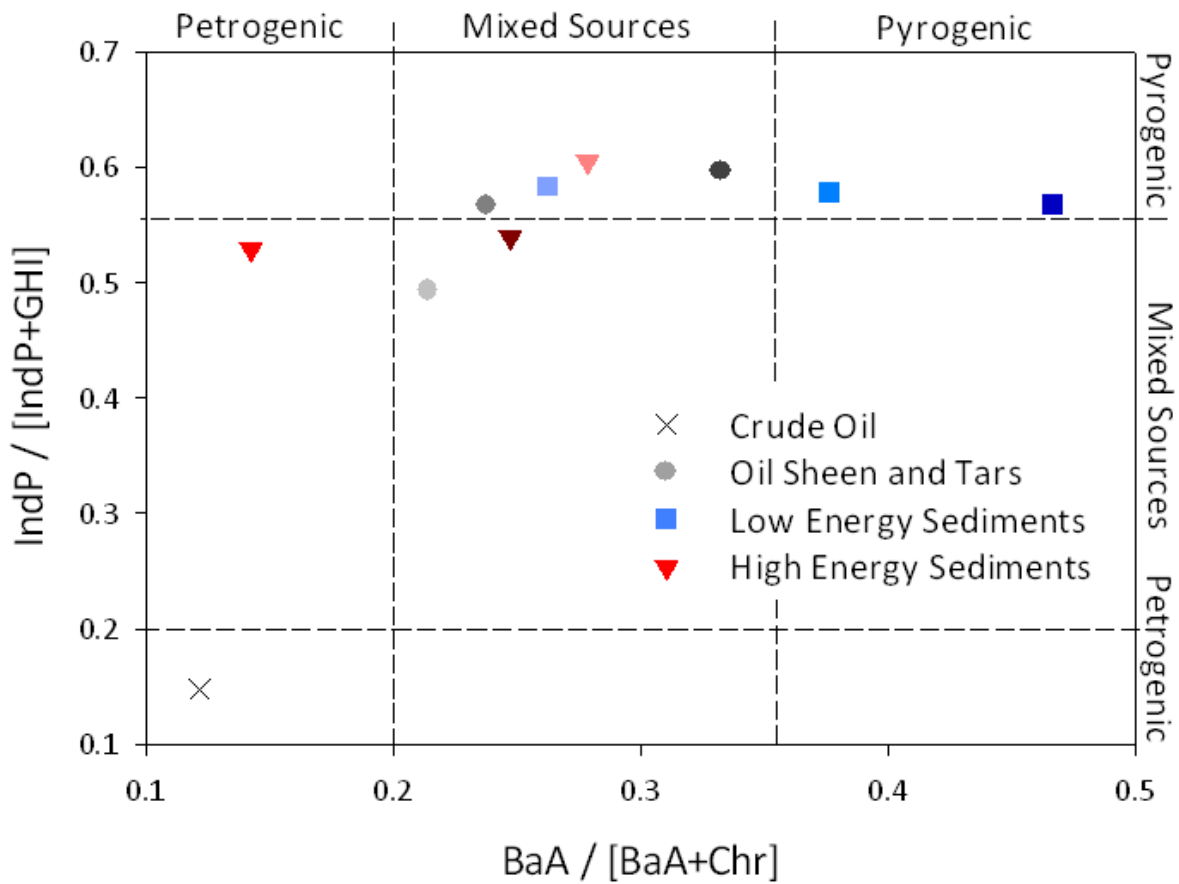
Figure 1.5 Two different PAH ratios are used to determine if the hydrocarbon pollution in samples originated from petrogenic, pyrogenic, or mixed sources. Shape of data point indicates sample type (detailed in legend). Low energy sediments include the bay sediment collected after 694 d, as well as the two low energy Grand Isle sediments collected after 88 d and 678 d. The shade of data point color indicates collection date, where the lightest shade is the earliest collection date, and the darkest is the latest collection date. Crude oil is the only sample that is predominantly petrogenic. All other samples show mixed or pyrogenic source. Sediment collected from the bay after 694 d is the furthest right sample, and has a highly pyrogenic signature.
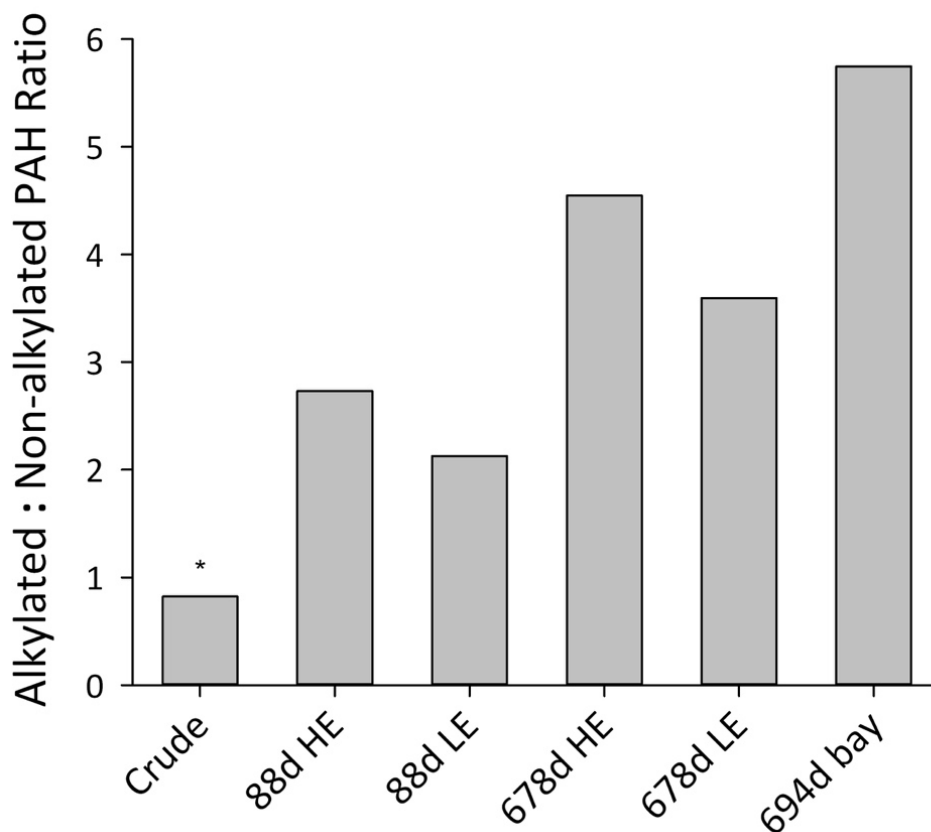
Figure 1.6. The ratios of alkylated PAHs : non-alkylated PAHs for oiled sediment samples. Samples labeled by collection date and site (high energy = HE, low energy = LE). This ratio is used as a proxy for weathering, as weathering will preferentially degrade non-alkylated PAHs over their alkylated homologues. We see crude oil has the lowest relative proportion of alkylated PAHs, suggesting little weathering (p=0.0105). Of sediments collected on Grand Isle, LA, the low energy sites have a lower ratio than high energy sites. The 694 d bay site, however, has the highest ratio, suggesting highest weathering degree.

Chapter 2. Streamlining and Expanding Environmental Petroleum Pollution Analysis using Ramped Pyrolysis – Gas Chromatography – Mass Spectrometry

ABSTRACT

In the aftermath of the *Deepwater Horizon* oil spill, many studies have investigated the chemical weathering of crude oil in the marine environment. This research is crucial, as these chemical changes dictate the toxicity and lability of petroleum hydrocarbons to marine species. There is a serious limitation, however, whereby analytical techniques cannot always identify the wide breadth of petroleum and petroleum-derived compounds. We explore the analytical capabilities of ramped pyrolysis – gas chromatography – mass spectrometry (Py-GC-MS) to evaluate environmental samples of petroleum hydrocarbons. We show that bulk flow Py-GC-MS can quantify overall weathering degree of oil samples, and that thermal slicing Py-GC-MS can quantify specific petroleum hydrocarbons in the "quantification zone", as well as qualify changes in non-GC amenable petroleum hydrocarbons with weathering in the "structure zone". Using this line of inquiry, we observe traditional depletion of GC-amenable petroleum hydrocarbons with weathering. Our data also suggest an increase in high molecular weight petroleum fractions, oxygenated products and complexity of resin and asphaltene components with advanced weathering, particularly in oil sheen. This analysis not only elucidates weathering trends with current samples, but also illustrates the analytical capacity of this method for future petroleum hydrocarbon investigations.

INTRODUCTION

Between April and July 2010, the *Deepwater Horizon* oil spill released five million barrels of crude oil from the Macondo wellhead into the Gulf of Mexico.[3] This oil spill has inspired advanced research in many fields, including human health[63], coastal restoration[44], marine species effects[40,64], microbial ecology[32] and dispersion modeling.[65,66] Of particular importance are advances being made in petroleum chemistry, as the hydrocarbon chemistry ultimately drives environmental toxicity threats.

Tracking hydrocarbon pollution in marine environments, however, is complicated by environmental weathering processes, which manipulate the chemical composition of oil over time and space.[7,10] In addition, due to the complexity of petroleum hydrocarbons, only a small fraction of the oil components can be quantified by traditional analytical techniques such as gas chromatography flame ionization detection (GC-FID) and GC-mass spectrometry (GC-MS). Of the four categorizations of petroleum hydrocarbons (saturated, aromatic, resins and asphaltenes), only a portion of saturated and aromatic hydrocarbons are GC-amenable, which is less than ~25% of Macondo crude oil.[22] Table 2.1 summarizes many of the analytical techniques and analytes that have been used to study petroleum chemistry following the *Deepwater Horizon* spill. The application of Fourier transform ion cyclotron resonance mass spectrometry (FTICR-MS) greatly expanded this analytical window by identifying numerous molecular formulas, such those containing oxygen and high molecular weight (HMW) compounds.[34,67] Although advanced technologies such as this have been employed, there is a large dependence on traditional instrumentation and an analytical window that largely excludes asphaltenes,

resins and chemically altered petroleum hydrocarbons, which are often the dominant fraction of highly weathered oil.[6,67]

To expand the analytical window, we investigated the analytical capacities of ramped pyrolysis – gas chromatography – mass spectrometry (Py-GC-MS). Traditionally, there are two types of analytical pyrolysis: (1) bulk pyrolysis, which steadily heats a sample and simultaneously measures gaseous output[68,69] and (2) cold-trapping or thermal slicing pyrolysis, which specifically analyzes the gaseous output of bulk pyrolysis within specific temperature ranges.[70,71] Recently, thermal desorption - flash pyrolysis has been employed, where a sample is rapidly heated to ~350°C and analyzed as the thermal desorption zone, and then the sample is heated to >600°C and analyzed as the pyrolysis zone.[72,73] These are all powerful tools that have been used since the mid-eighteenth century for investigations of many topics, including fossil fuel kinetics[69,71], soil organic matter[74] and more recently, radiocarbon dating[75], plastic polymer identification[76] and polycyclic aromatic hydrocarbon (PAH) identification in marine waters[72,73]. These lines of investigation, however, do not quantify specific hydrocarbons, nor do they investigate chemical composition changes of marine oil spills during the weathering. Pendergraft and Rosenheim (2014) used ramped pyrolysis to specifically evaluate oiled sediment and tar from the *Deepwater Horizon* spill[77]. Their bulk flow pyrolysis technique heats organic material in a constant stream of He, oxidizes the flushed products by mixing in O_2, and collects the resulting CO_2 for isotopic analysis over different temperature intervals. They tracked the CO_2 evolution with temperature to draw conclusions about the thermochemical stability of organic material in oiled samples. They

also analyzed the emitted gas for petrocarbon (^{14}C) signature and found that all samples had highly depleted ^{14}C, which indicates that they were contaminated by petrochemical sources. However, there is a need to evaluate oil weathering from a molecular level to gain clear insights into how oil components evolve with weathering.

Here, our goal is to use ramped pyrolysis to evaluate (a) overall weathering degree of polluted environmental samples, (b) compound-specific quantification of petroleum hydrocarbons, (c) recalcitrance of petroleum hydrocarbons with weathering and (d) relative content of non-GC amenable hydrocarbons. Using oiled samples collected by Pendergraft and Rosenheim, 2014,[77] we demonstrate that bulk Py-GC-MS yields a holistic view of petroleum hydrocarbon weathering, which streamlines the traditional analysis processes requiring sample preparation and fractionation. Thermal slicing Py-GC-MS allows quantification of GC-amenable petroleum hydrocarbons within the low temperature (50-370°C) pyrolysis zone, or the "quantification zone", where multiple analytes are measured at one time without sample preparation. Thermal slicing Py-GC-MS also provides insight into the recalcitrance of petroleum hydrocarbons with weathering, as revealed by thermal characterization and the relative content of HMW and oxygenated hydrocarbons during high temperature (370-650°C) pyrolysis, or the "structure zone". Overall, this efficiently demonstrates depletion of traditionally GC amenable petroleum hydrocarbons with increased weathering, but retention of complex petroleum hydrocarbons such as oxygenated hydrocarbons, resins and asphaltenes, with novel method application.

MATERIALS AND METHODS

Sample Collection

Oil samples were collected in conjunction with Pendergraft and Rosenheim,

2014,[39] including surface oil sheen, oiled sediment and tar resulting from the *Deepwater*

Horizon spill. All samples were opportunistically collected within 881 days of the

wellhead blowout (20 April 2010) on Grand Isle or within Bay Jimmy, Louisiana

(29.258°N 89.958°W and 29.477°N 89.894°W, respectively). Samples were collected in

pre-combusted glassware and immediately frozen for storage. Prior to analysis, an

aliquot of each tar sample was freeze-dried using a Labconco FreeZone 2.5 Plus. In

addition, oil from the Macondo well was obtained from the National Institute of Science

and Technology (NIST) and analyzed for comparison to weathered samples.

Bulk Py-GC-MS

Analysis was completed using a multi-shot pyrolyzer (model EGA/PY-3030D,

Frontier Laboratories Ltd.), attached to a GC-MS (Shimadzu GCMS-QP2010 Plus). For

bulk analysis, ~0.1 mg freeze-dried sample was weighed in a deactivated, stainless steel

sample cup. The cup was dropped into the pyrolyzer furnace from the automatic sampling

carousel and heated from 50-800°C at a ramp of 20°C min^{-1}. During heating, the

volatilized, gaseous material was simultaneously eluted into a short GC column (Frontier

Lab Ultra ALLOY EGA Tube; length 2.5m; I.D. 0.15 mm; O.D. 0.47 mm) in a 1 mL

min^{-1} helium flow. The GC injection port and oven temperatures were held constant at

300°C. MS analysis was completed with ion source temperature of 230°C, detector

temperature of 320°C and scanning ion range of m/z 26-600. The results of this analysis

yielded a smooth pyrogram curve, which measures total ion output as a function of

pyrolysis temperature.

Thermal Slicing Py-GC-MS

Freeze-dried samples were weighed (~0.1mg) in deactivated, stainless steel

sample cups and loaded onto the pyrolyzer auto-sampler. Samples were heated six times

per sample, in a series of pre-programed thermal slices: 50-90, 90-170, 170-290, 290-

370, 370-530 and 530-650°C. These ranges were selected because they provide good

separation of common petroleum hydrocarbons from bulk pyrograms in our preliminary

runs; however, any desired thermal slicing program could be designated depending on the

sample type. Before the sample was pyrolyzed, the second inch of the GC column was

cooled externally to -190°C by a flow of N_2 gas, which had been cooled by flowing

through a dewar of liquid N_2. As the sample was heated from 50-90°C the sublimated

material was trapped where the GC column was cooled. After heating to 90°C, the

sample was ejected from the pyrolyzer (but held within the auto-sampling system) so that

it stopped heating, the cryogenic cooling system turned off, and the pyrolyzed material

eluded through the GC column (Frontier Lab 30 m Ultra ALLOY Capillary Column, I.D.

0.25 mm and Film 0.25 μm) in a 1mL min^{-1} helium flow. The GC oven temperature

program started when the cryogenic system turned off, maintaining 40°C for 2 minutes,

ramping at 10°C min^{-1} to 150°C, ramping at 20°C min^{-1} to 320°C and holding 320°C for 3

minutes. The GC inlet temperature and MS parameters were the same as bulk pyrolysis,

with the exception that a Selective Ion Method (SIM) was employed to target specific

analytes (Table B.1). After GC-MS analysis of the first thermal slice, the column was

cooled again, the sample was dropped back into the pyrolyzer and the process repeated

for all desired thermal ranges, taking ~5 h for one sample.

The analyte peaks were identified based on retention time by comparison to

authentic standards. For quantification, the sum of each thermal slice was compared to a

three-point standard curve, quantified with the same summation of slices technique. Each

sample was run in triplicate. During pyrolysis, low molecular weight (LMW) compounds

in solvent can volatilize easily, which makes it difficult to obtain a consistent output for

compounds with a carbon backbone under ~18 carbons in length. We are able to lessen

this issue by stabilizing LMW n-alkane, PAH and alkylated PAH standards with solvent-

dissolved polystyrene, which creates a matrix around the compound and stabilizes it for

analysis. All C_9-C_{20} alkane, PAH and alkylated PAH standard curves and concentrations

of crude oil used this stabilization technique. The system is not completely devoid of

oxygen, so when quantifying CO_2 we average the CO_2 results of multiple blanks and

subtract this from the CO_2 content in samples.

Traditional Chemical Analysis

Each sample was analyzed for n-alkanes, PAHs, alkylated PAHs, hopanes and

steranes following the procedure by Liu et al. (2012),[7] as detailed in Chapter 1. Briefly,

~1 g of sample was weighed and extracted with dichloromethane for 24 h using Soxhlet

extraction. Prior to extraction, samples were spiked with deuterated standards:

hexadecane-d$_{34}$, fluorine-d$_{10}$ and benzo(e)pyrene-d$_{12}$. Sample fractionation followed

procedures in Wang et al. (2004)[42], where samples were fractioned in a column packed

with 3 g activated silica gel and topped with 3-5 g anhydrous sodium sulfate. Following

column conditioning with 20 mL hexanes, saturated hydrocarbons were eluted and collected with 12 mL of hexanes, followed by aromatic hydrocarbon elution and collection in 15 mL of hexanes and benzenes (1:1). These fractions were concentrated with Rotovap to a final volume of 100 μL. Total GC-detectable saturated n-alkanes were analyzed using GC-MS (Shimadzu GCMS-QP2010 Plus). Total PAHs and alkylated PAHs were analyzed using GC-FID (Shimadzu GC-2014). A four-point standard curve with internal standard calibration was used for quantification. Spikes were used to adjust for percent recovery. All solvents were chromatographic grade and purchased from either Fisher Scientific or Sigma-Aldrich. Recalcitrant Macondo biomarker ratio 17α(H)-22,29,30-trisnorhopane:17α(H),21β(H)-hopane[18] was calculated using both thermal slicing Py-GC-MS and traditional analysis to confirm *Deepwater Horizon* source (Figure B.1).

RESULTS

Bulk Py-GC-MS

The crude oil showed highest sublimation at low temperatures (<300°C) (Figure 2.1) due to the dominance of LMW compounds.[6] After 46 d of weathering, the pyrogram shifted to the right and there is a further shift in oiled sediment collected after 88 d. Tar samples collected 337 d and 881 d following the spill became relatively more concentrated with compounds with higher boiling points or HMW. Moreover, the pyrograms only differ slightly between 337 d and 881 d tar. Additional pyrograms of oiled sediment were omitted from this Figure 2.1 because of their extremely low overall ion content.

To quantify these patterns, we integrated the content volatilized within the low and high temperature zones. The integration of the first pyrogram peak (i.e. labile component) was divided by the integration of the second pyrogram peak (i.e. recalcitrant component), as the peak ratio (equation 2.1). Peak areas were calculated as the integrated total ion count (TIC) from pyrogram start to lowest trough for peak 1, and lowest trough to end of pyrogram for peak 2. For example, one replicate of the 46 d oil sheen sample had the lowest point at 364.9°C, so peak 1 is the TIC integration from 50-364.9°C and peak 2 is the TIC integration from 364.9-800°C.

$$(2.1) \text{ Peak Ratio} = \frac{\Sigma \text{ TIC Peak 1}}{\Sigma \text{ TIC Peak 2}}$$

We then used traditional chemical analysis to quantify the total n-alkane, PAH and alkylated PAH content, normalized to recalcitrant internal standard $17\alpha(H),21\beta(H)$-Hopane[16] (C_{30}-hopane) for comparison. The increase in peak ratios from pyrograms aligns well with increased measured hydrocarbon content (Figure 2.2), with the exception of tar samples, which had a relatively higher peak ratio than hydrocarbon content.

Thermal Slicing Py-GC-MS

In thermal slicing pyrolysis, organic compounds within a sample are separated by pyrolysis temperature ranges based on their volatility and thermochemical stability, and compound-specific chromatographic separation is further achieved based on polarity and molecular weight, as in traditional GC analysis. The result of this analysis is six chromatograms (one for each thermal slice), each of which measures ion count as a function of GC elution time, seen in Figures 2.3 and 2.4 for Crude Oil and 337 d tar,

respectively. As expected, the overall detected content is higher in crude oil than in 337 d tar, as illustrated by the TIC scale (Figures 2.3 & 2.4). Peaks at low retention time (i.e., LMW compounds) dominated in the low temperature range of 50-90°C (Figures 2.3A and 2.4A). Detected peaks shift to higher retention times as pyrolysis temperature increases, illustrating that higher pyrolysis temperatures are required to volatilize HMW compounds. In general, fewer peaks are detected in high temperature zones (370-650°C; 2.3E, 2.3F, 2.4E, 2.4F) than low temperature zones and no compounds are detected past 650°C. The two high temperature zones also show compound cracking, as evidenced by peak pairs of alkene followed by alkane, highlighted in the zoomed insets of Figures 2.3E and 2.4E. There is also an increase in CO_2 peak areas (retention time 2.00 m; m/z = 44) in the last two thermal slices.

Within the first four thermal slices (50-370°C) peaks for targeted *n*-alkanes, PAHs, alkylated PAHs, hopanes, and steranes were quantified. These thermal slices are referred to as the "quantification zone", as these slices were used to quantify the concentration of target analytes and no significant cracking occurred. To validate these concentrations, we compared them to the concentration achieved by traditional wet chemical analysis (Figure 2.5). Quantifications are normalized to C_{30}-hopane. The pyrolysis results are higher than traditional analysis results (Figure 2.5). For example, absolute concentrations for crude oil Py-GC-MS ΣPAH = 22,740 ng mg^{-1} and Σ*n*-alkanes (C_{20}-C_{37}) = 132,094 ng mg^{-1} while traditional analysis results are 5,887 ng mg^{-1} and 75,596 ng mg^{-1}, respectively. For 337 d tar, Py-GC-MS ΣPAH = 4,347 ng mg^{-1}, Σ*n*-

alkanes (C_9-C_{37}) = 226 ng mg^{-1}, and traditional analysis results are 1,397.9 ng mg^{-1} and 113.6 ng mg^{-1}, respectively.

The relative contribution for detected hydrocarbons from the quantification zone was not equal between the four thermal slices, as illustrated by the percent each thermal slice contributed to total detected n-alkane in crude oil (Figure 2.6). In the crude oil, the majority of detected n-alkanes eluded between 170-290°C and longer chains required higher temperatures (Figure 2.6A). Relative to the crude oil, oil sheen and tar samples have increased compound contribution from higher thermal ranges (Figure 2.6B-D). For example, C_{25} in crude oil eluded ~20% between 90-170°C and ~80% between 170-290°C, but in 337 d tar it eluded ~8% between 90-170°C and ~92% between 170-290°C. In addition, C_{26-33}-alkanes in tar samples required higher temperature to volatilize for analysis than in crude oil or oil sheen. Therefore, higher temperature is required to sublimate the same compounds for analysis in more weathered samples.

While the quantification zone of thermal slicing Py-GC-MS encompasses all traditionally GC amenable compounds, the two high temperature thermal slices (370-650°C), defined as the structure zone, can provide information on the thermally stable components (presumably dominated by HMW). In these thermal slices, substantial compound cracking was observed, which may be a result of side-chain cleavage of asphaltenes or resins or decarboxylation of oxygenated hydrocarbons[78–80]. Although we cannot directly identify the parent compounds, we can compare product patterns between samples. Peak areas of n-alkanes from the structure zone, normalized to C_{30}-hopane and sample weight, were compared between all samples, focusing on crude oil, oil sheen and

tar (Figure 2.7). The total n-alkane content in oil sheen is ~2 times that of crude oil, where n-alkanes $<C_{18}$ and $>C_{30}$ show the most pronounced differences and those between C_{18}-C_{30} are closer in concentration. Both crude oil and oil sheen have higher structure zone n-alkanes content than weathered tars, in which total alkane is ~4 times higher in crude oil than both tar samples, but there are more HMW n-alkanes C_{30}-C_{33} in tar than crude oil. A significant amount of LMW PAHs and alkylated PAHs were detected in the structure zone (normalized to C_{30}-hopane and sample weight), but only phenanthrene, fluoranthene and pyrene were detected in crude oil (Figure 2.8). Oil sheen has the highest total content, which is approximately 1.5 times higher than 227 d tar, 4 times higher than 881 d tar and 7 times higher than crude oil. Thus, tar samples show similarly high content compared to crude oil. These compounds are presumably a result of charring of organic material[81,82] or a product of HMW compound cracking,[80] which will be further discussed later.

A final insight drawn from the structure zone is the presence of oxygenated hydrocarbon. An increase in the CO_2 peak with pyrolysis temperature can be seen in crude and tar samples (Figures 2.3 and 2.4; retention time 2.00 min), which is likely a result of cracking of oxygenated hydrocarbon through reactions such as decarboxylation. CO peaks are also detected but minimal, thus we focus on CO_2. CO_2 peaks were summed for each thermal slice and blank CO_2 values were subtracted, but the values in the quantification zone were almost equal to the blanks, so total CO_2 reported is primarily from the structure zone. Crude oil and 337 d sediment (which was collected from the buried, oiled sediment layer) show no significant C_{30}-hopane normalized CO_2 content, but

46 d oil sheen and 337 d tar show very high CO_2 content, approximately six orders of magnitude higher (Figure 2.9). We compare CO_2 content to the sum of n-alkanes and PAHs from the structure zone of all samples analyzed. There is a positive, linear correlation ($R^2 = 0.8179$; Figure B.2). Total content from structure zone, including CO_2, n-alkanes and PAHs can be found in Table B.2.

DISCUSSION

There are four operational categories of petroleum hydrocarbons: saturates, aromatics, resins and asphaltenes.[17] The GC-amenable portion encompasses LMW n-alkanes and aromatic compounds. Resins and asphaltenes are HMW, polar and have an extensive aromatic hydrocarbon backbone according to hypothetical models.[6,78,80] Comparatively, resins are more polar because they typically have a longer aliphatic tail extending off of this backbone structure.[6,83] The latter two categories are largely understudied, especially in relation to the *Deepwater Horizon* spill,[19,20] partially because their molecular complexity makes them difficult to characterize and quantify.[79,84]

Analytical pyrolysis has been used in the petroleum industry to study the thermal degradation of all four hydrocarbon classes. In these studies, cracking products of resins and asphaltenes consistently elude at high temperatures (~400-600°C), whereas the majority of saturated and aromatic hydrocarbons elude ~100-350°C.[69,85] Therefore, it is reasonable to assume that a large portion of detected peaks in the structure zone (370-650°C) are a result of resin, asphaltenes and some HMW aromatic decomposition, and simultaneously conclude that resins and asphaltenes are not interfering with the quantification zone. These previous analyses, however, are based on total organic matter

within a hydrocarbon fraction and do not detail compound-specific elution. This is important, considering that thermochemical stability is determined by the chemical structure and compound aggregations. For example, weathered asphaltenes are known to non-covalently aggregate and become encapsulated by the non-polar head of resin molecules, creating an aromatic, asphaltene sheet in the center surrounded by a layer of resins with the aliphatic tails arranged away from the center of the structure, called a micelle. These micelles are what stabilize petroleum flocculation because in sum, they are relatively less polar than the individual compounds.[6,84,86–88] Therefore, these aggregations may change the thermal response to pyrolysis in weathered petroleum compared to crude oil. In fact, much can be learned about the transformation of petroleum hydrocarbons in natural environments by comparing the pyrolysis patterns of weathered and un-weathered oil. Here, we use bulk and thermal slicing analysis to holistically expand insight on overall and compound-specific petroleum weathering.

Bulk Py-GC-MS to evaluate overall environmental weathering
During ramped pyrolysis, organic compounds sublimate based on their volatility and thermochemical stability, whereby the most stable compounds and compound aggregations require higher temperatures for analysis.[39,68,69] The observed pattern of right-shifted bulk pyrogram peaks with sample age or weathering, therefore, suggests a decrease in LMW compounds with time. This pattern is consistent with environmental weathering of oil, in which lighter, more volatile components are preferentially removed over time via processes such as evaporation, dissolution, or biodegradation.[2,7,10,12,13] The similarity between tar collected 337 d and 881 d following the spill is not surprising, as

tar is considered to be fairly recalcitrant upon formation and shows minimal chemical change with time.[20,89]

These pyrogram shapes correspond well to those reported by Pendergraft and Rosenheim, 2014,[39] which used the same set of samples but pyrolyzed them at a slower ramp (5°C min^{-1}). They observed nearly identical pyrogram shapes and the same pattern of right-shifted peaks in older samples, confirming reproducibility of the pyrogram shapes. They too attributed these shifts to increased weathering. In order to confirm this, they compared PAH content to ^{14}C content, illustrating that least-weathered samples had highest PAH content and highly depleted [14]C (petrogenic source).[58] In sum, this illustrates overall petroleum weathering patterns where total petroleum hydrocarbon materials, particularly labile, LMW compounds, decrease with time. This also corresponds to previously mentioned pyrolysis studies, which found that saturated and aromatic hydrocarbons had peak elution ~100-350°C.[69,85]

We expanded this analysis to compare pyrogram peak area to total GC-amenable hydrocarbon content. GC-amenable hydrocarbons correlate to a high peak ratio and there is an overall decrease in peak ratio with increased weathering (Figure 2.2). This confirms that thermochemical stability does correlate with temperature, whereby low temperature zones are dominated by LMW, GC-amenable hydrocarbons and weathering decreases this hydrocarbon content. There is a deviation, however, where peak ratios of tar samples are relatively higher than measured hydrocarbon contents. This is likely due to presence of LMW hydrocarbons in tar that are not typically GC-amenable, such as oxygenated hydrocarbons, which have recently been found to be a dominant portion of tar

aggregations[19,34] or aggregations of aliphatic hydrocarbons called nucleations that can be trapped within micelles, requiring higher volatilization temperatures than Soxhlet extraction used in the wet chemical analysis.[90,91] Bulk pyrolysis does not exclude these compounds from analysis, yielding a more holistic view of weathering that effectively highlights the difference between tar and oiled sediment. Overall, this expands previous work to detail a semi-quantitative way to measure weathering using bulk pyrolysis peak ratios, which is an advantage compared to time-consuming traditional analysis techniques that involve sample extraction, cleaning and fractionation.

Thermal Slicing Py-GC-MS for compound quantification

Within the quantification zone, we were able to quantify concentrations of traditional GC-amenable hydrocarbons in samples with significant petroleum pollution. Our concentrations are higher than those using wet-chemical analysis. Pyrolysis could be more efficient at extracting total petroleum hydrocarbons in weathered samples, as the sample preparation in wet-chemical analysis involves multiple points of extraction and fractionation where organic material could be lost. Particularly *n*-alkanes, which elute in the first fraction during chromatographic column separation, can be 20-30% lost to the second fraction in an attempt to avoid losing aromatic hydrocarbons from the second fraction.[92,93] In addition, the tar matrix is complex, as previously described, and matrices have been shown to affect quantification of PAHs in marine samples, whereby the quantification is highly dependent upon how labile the analyte is in the sample matrix and extraction solvent.[93,94] Here, thermal extraction may be more comprehensive than solvent extraction. Typically, surrogate spiking corrects for these matrix effects in GC-MS

48

analysis[28,95]; however, these corrections may not be completely accurate because the spike is added to the outside of the sample and thus, not integrated into the sample matrix. Finally, although we use the same GC-MS for traditional analysis and pyrolysis analysis, we highlight that quantification differences are expected between different analysis systems, such as GC-MS, GC-FID and GCxGC.[93,96]

An alternative argument is that pyrolysis creates additional hydrocarbons from cracking and charring. Cracking is thought to occur at weak points in compound aggregations, primarily heteroatoms, or a non-carbon component of an aromatic ring.[85,97] This can yield aliphatic products from tail cracking, manifested as alkene, alkane peak pairs (Figure 2.3E & 2.4E),[78,86] or cracking of the backbone structure itself, leading to formation of LMW aromatic hydrocarbons.[86,98] However, compound cracking rarely occurs in the quantification zone, as evidenced by few alkene peaks. In addition, Williams et al. (2014) showed that charring occurs primarily between 300-450°C from ramped pyrolysis and is not re-volatilized for analysis, but remains within the sample container.[99] The majority of PAHs and alkylated homologues were detected under 300°C. In fact, our quantification zone temperature is not much higher than injection port temperatures (~300°C[17]) commonly observed in most GC analysis; therefore, temperature is not likely a confounding factor in our quantification results.

Thermochemical stability insight from the quantification zone

The thermal distribution of quantified compounds provides insights into the matrix of weathered oil. Weathered samples require a higher temperature to be volatilized for analysis than crude oil, as demonstrated by *n*-alkane distribution in Figure 2.6. In

pyrolysis literature, sublimation is thought to be controlled by activation energy.[69,71,99] Although the specific activation energy under our pyrolysis parameters cannot be quantified (it would require homogenous analyte or multiple heat ramping experiments), the thermal distribution of compounds represents how specific petroleum hydrocarbon activation energies change as a result of environmental weathering. We show that the thermal nature of petroleum with weathering moves from less to more thermally stable, particularly with the formation of tar. A likely explanation for this shift is that paraffin nucleation creates more recalcitrant hydrocarbon matrices, as previously discussed.[90,91] This nucleation allows even LMW compounds to increase in stability with time, thus higher temperature is required to extract these compounds for analysis. It is interesting to note that C_{26-33}-alkanes required higher temperatures to volatilize in tar samples compared to crude oil or oil sheen, which may be a result of nucleation of alkanes of this molecular weight range. To our knowledge, this is the first time that the thermal stability of weathered oil has been illustrated on a compound-specific level.

Complex Compound Insight from the Structure Zone

By comparison to traditional analysis, we have confirmed that all GC-amenable petroleum hydrocarbons were detected and quantified within the quantification zone. Therefore, the *n*-alkanes and LMW aromatics detected within the structure zone were from charring and/or cracking of the HMW hydrocarbons. As previously discussed, there is little evidence to support detection of char using ramped pyrolysis, but rather formation of char within the sample container.[99] Cracking of HMW aliphatic, resins, asphaltenes or oxygenated hydrocarbons could lead to the formation of alkanes (via cracking of side

50

chains or oxygenated tails) or aromatics (via cracking the backbone structure of asphaltenes/resins or cleaving the oxygenated tail of oxygenated PAHs). Although we cannot specifically distinguish between these sources, we can make inferences about their content based on these cracking products.

Overall, we observed an increase in PAHs and alkylated PAHs detected in the structure zone with increased weathering. Detected *n*-alkanes were higher in crude oil than tar, but oil sheen had the highest structure zone hydrocarbon content for *n*-alkanes and PAHs. Simultaneously, we observe a clear increase in CO_2 in the structure zone. In the quantification zone, CO_2 is approximately equal to blank runs and thus, negligible. The majority, if not all, of the CO_2 content illustrated in Figure 9 is from the structure zone, with almost equal contribution from both structure zone slices. We hypothesize that this is from high-temperature decarboxylation of oxygenated hydrocarbons, a predominant byproduct of petroleum weathering.[21,100,101] Oxygenated hydrocarbons derive from photooxidation and biodegradation processes,[22] whereby highly polar species, such as carboxylic acid and ketones, are formed.[21,22,34,67] This would explain why the surface oil sheen, which had maximum UV exposure, has the highest CO_2 content of our samples. Recent studies suggest that oxygenated hydrocarbons help stabilize tar matricies,[19,34] which explains the high content in the 337 d tar sample. Similarly, the relatively low 881 d tar CO_2 content suggests that this particular sample may have undergone less photooxidation, possibly via sub-surface formation, or that oxygenated species had been degraded with time. If cracking in the structure zone is from decarboxylation of oxygenated hydrocarbons, we would expect to see structure zone

51

hydrocarbon content to follow the same pattern as CO_2, whereby oil sheen has the highest content, followed by 337 d tar. This is the pattern we observe, confirmed by a positive correlation between structure zone hydrocarbon content and CO_2 values (Figure B.2; $R^2 =$ 0.8179), suggesting that high temperature pyrolysis does indeed cleave oxygenated hydrocarbons, leading to detection of LMW hydrocarbons in the structure zone.

We cannot, however, eliminate the option that structure zone hydrocarbons are from the cracking of HMW hydrocarbons (i.e. resins and asphaltenes), not just oxygenated hydrocarbons. This is particularly relevant because the majority of oxygenated hydrocarbon precursors are aliphatic, which explains increased *n*-alkane and alkene content, but not PAH content.[21,22] Therefore, an increase in aromatic cracking products is likely attributable to an increase in resin and asphaltene components, which have extensively aromatic backbones. This is supported by FT-ICR analysis that suggest a decrease in overall PAH content (including oxygenated species) but an increase in overall HMW hydrocarbon complexity with weathering.[34] Ruddy et al. (2014) also elegantly pointed out that heteroatom changes in HMW hydrocarbons could be contributing to this complexity.[34] Interestingly, these heteroatoms, which are the location of high temperature cracking, are largely converting from pyridinic-nitrogen-containing species to oxygen-containing species, primarily ketones. Therefore, although the increased aromatic content at high temperature may not be a result of traditional oxidation of side chains (predominantly observed in saturates), it may be from oxidation of heteroatoms, meaning oxidation destabilized the asphaltene/resin matrix leading to cracking of HMW asphaltenes and resins.

To our knowledge, this is the first comparison of high temperature cracking products of weathered and un-weathered petroleum. We observe an increase in compound complexity with weathering, particularly of oil sheen, attributable to side chain oxidation of saturates and increase of resins and asphaltene cracking products, possibly from increased complexity with addition of oxygen-containing heteroatoms. This corroborates our prior interpretation that weathering increases thermochemical stability, because oxidized product aggregations and micelles increase stability. Although we cannot detail specific parent molecules, thermal slicing Py-GC-MS does allow for novel comparison of complex hydrocarbon species between environmental samples in a simple, efficient manner.

IMPLICATIONS

Py-GC-MS provides a multi-faceted approach to evaluating environmental petroleum pollution. Here we have demonstrated the capacity for (1) bulk pyrolysis to evaluate overall weathering degree and (2) thermal slicing pyrolysis to quantify GC amenable petroleum hydrocarbons and qualify weathering of non-GC amenable components. We found an overall decrease in the content of GC amenable petroleum hydrocarbons with environmental weathering following the *Deepwater Horizon* oil spill. Conversely, we observed a relative increase in cracking products created in the high-temperature structure zone, implying a relative increase in non-GC amenable compounds with time. This could include HMW compounds, resins, asphaltenes, and oxygenated hydrocarbon species, all of which are more thermally stable and require high

temperatures to be cracked for analysis. These complex hydrocarbons have not been the focus of traditional toxicity studies, but are important to monitor as they are persisting long after GC amenable saturates and aromatics, and potentially becoming more bioavailable with increased oxidation. Future work includes expansion of Py-GC-MS to quantify, not just qualify, the oxygenated hydrocarbon content. Overall, Py-GC-MS is an extremely efficient tool for characterizing petroleum pollutants in environmental samples, within and beyond the traditional analytical window.

Table 2.1 Summary of analysis techniques and the target analytes investigated in studies pertaining to weathering of crude oil following the *Deepwater Horizon* oil spill. All analysis techniques require wet-chemical sample preparation,with the exception of techniques denoted with †. All analytes are compounds found in source oil, with the exception of analytes denoted with a *, which are considered to be weathering products.

Analysis Technique	Target Analyte

Gas Chromatography - Mass Spectrometry (GC-MS)	Aromatic hydrocarbons:
	  PAHs and Alkylated PAHs[2,7,9,10,14,22,43,102]
	  BTEX[2,7,9,10,22,102]
	  Alkylated benzenes[2,7,10,22]
	Petroleum biomarkers[2,7,10,14,22,43]

Gas Chromatography - Flame Ionization Detection (GC-FID)	Total solvent extractable saturated hydrocarbons[2,7,10,22,102,103]
Comprehensive two dimensional GC (GCxGC)	Saturated hydrocarbons[2,18,21,22,31,34,103] Petroleum biomarkers[18,21,22,31,34,103]
Thin Layer Chromatography - Flame Ionization Detection (TLC-FID)	Saturated, aromatic and oxygenated* fractions (not compound- specific)[22]
Fourier Transform Infrared Spectroscopy (FT-IR)	Oxygenated hydrocarbons by functional group*[22]
Environmentally Persistent free Radical (EPR) Spectrometry	Organic free radicals (asphaltene, tar or oxygenated hydrocarbon* derived)[20] Transition metal ions[20]
Ultrahigh resolution Fourier Transform Ion Cyclotron Resonance Mass Spectrometry (FTICR-MS)†	Saturated, aromatics and polar*[34] hydrocarbons (including low and high molecular weight fraction to ~C100)[34,67]
Inductively Coupled Plasma - Mass Spectrometry (ICP-MS)	Trace Metals[7]
Elemental Analyzer–Isotope Ratio Mass Spectrometer (EA–IRMS)	Asphaltenes[19]
Airborne Visible/InfraRed Imaging Spectrometer (AVIRIS)†	Total surface oil[104]
Ramped Pyrolysis†	Radiocarbon (^{14}C) content[39,58]
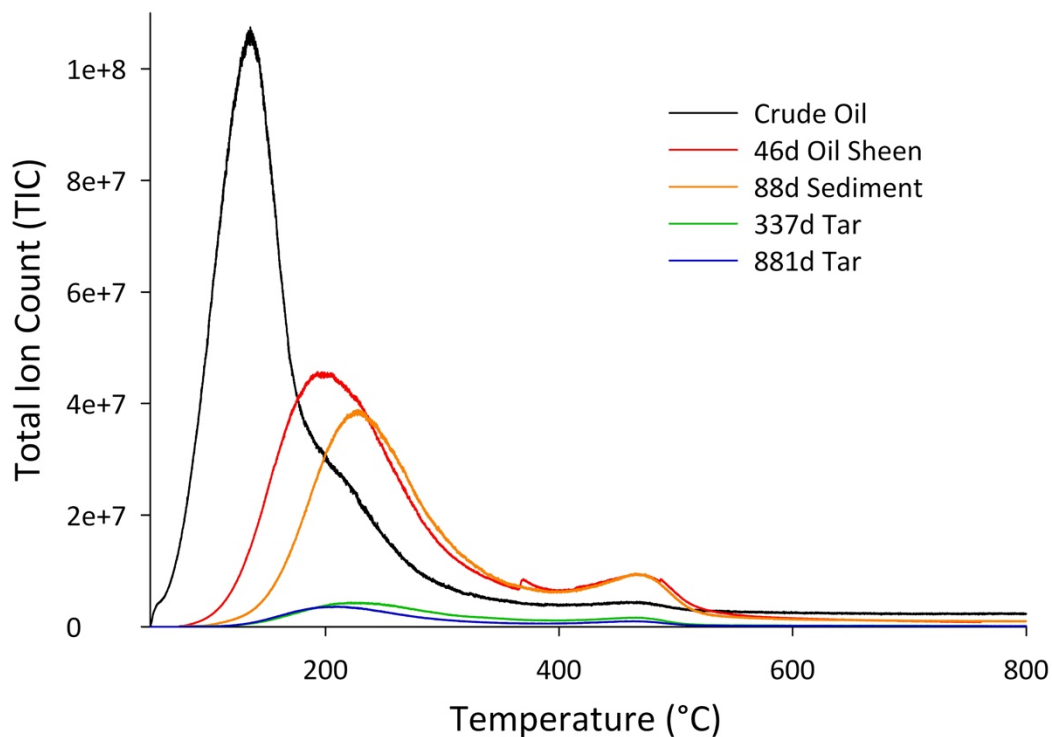
Figure 2.1 Bulk pyrograms for five different samples are overlaid to illustrate the relationship between pyrogram shape, collection date and sample type. All pyrograms were normalized to the weight of sample pyrolyzed. Samples that spent more time in the environment (i.e. up to 881 d post-spill) have overall less material (total ion count; TIC) and peaks are shifted towards higher temperatures. (46 d oil sheen n=2; all other samples n=3.)
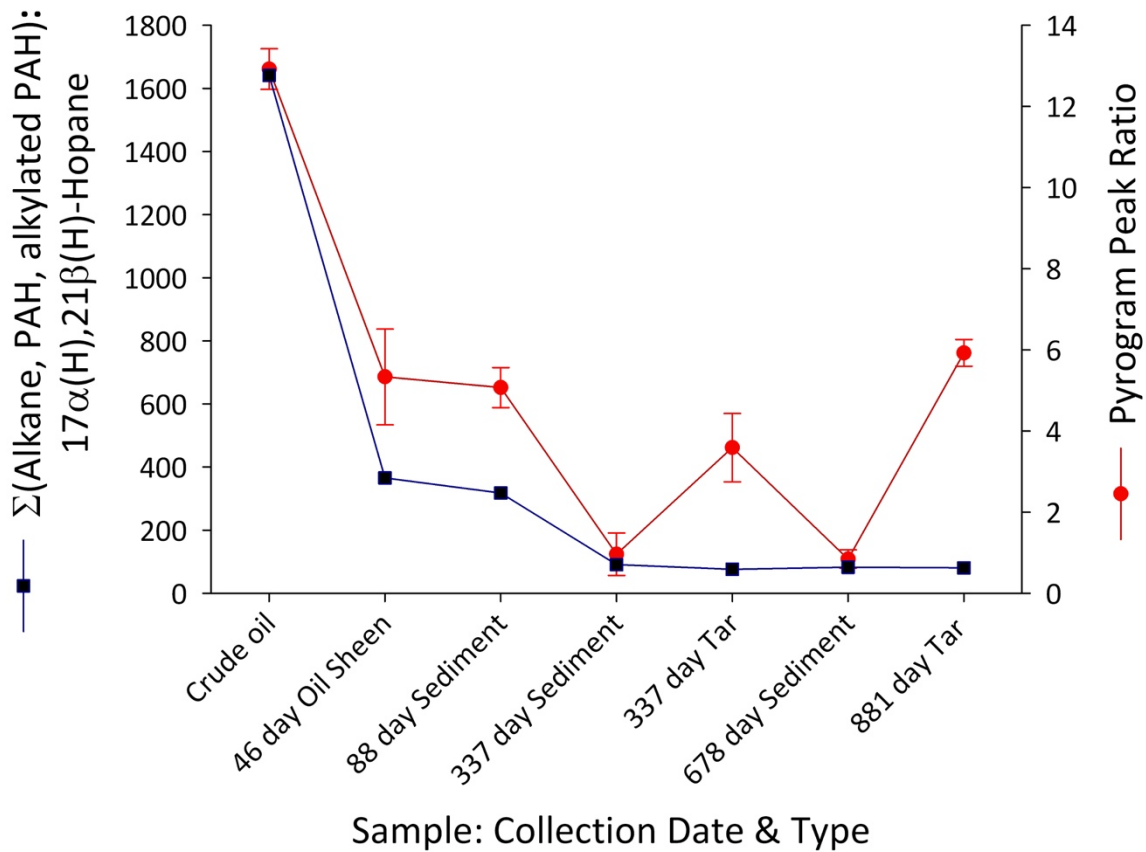
Figure 2.2 Peak ratio generated from bulk pyrograms is compared to the sum of analyzed *n*-alkanes, PAHs and alkylated PAHs, normalized to recalcitrant internal biomarker C_{30}-hopane. We observe highest peak ratio and hydrocarbon content in crude oil. With time, both values decrease in a corresponding pattern. Exceptions include tar samples, whereby the pyrogram peak ratio is higher than detected GC-amenable content. Peak ratio bars represent standard error (*n=3*).

Figure 2.3 Six chromatograms are shown for each thermal slice of a crude oil sample, generated using thermal slicing Py-GC-MS. Note that the y-axis scale changes between slices, a result of varying content elution with temperature. The zoomed portion of Figure E is used to highlight the occurrence of thermal cracking. The peaks at ~5.5 minutes in all slices and the peak at ~7 minutes in 3E is a result of polystyrene, which was used to stabilize this solvent-dissolved crude oil sample for analysis.

58

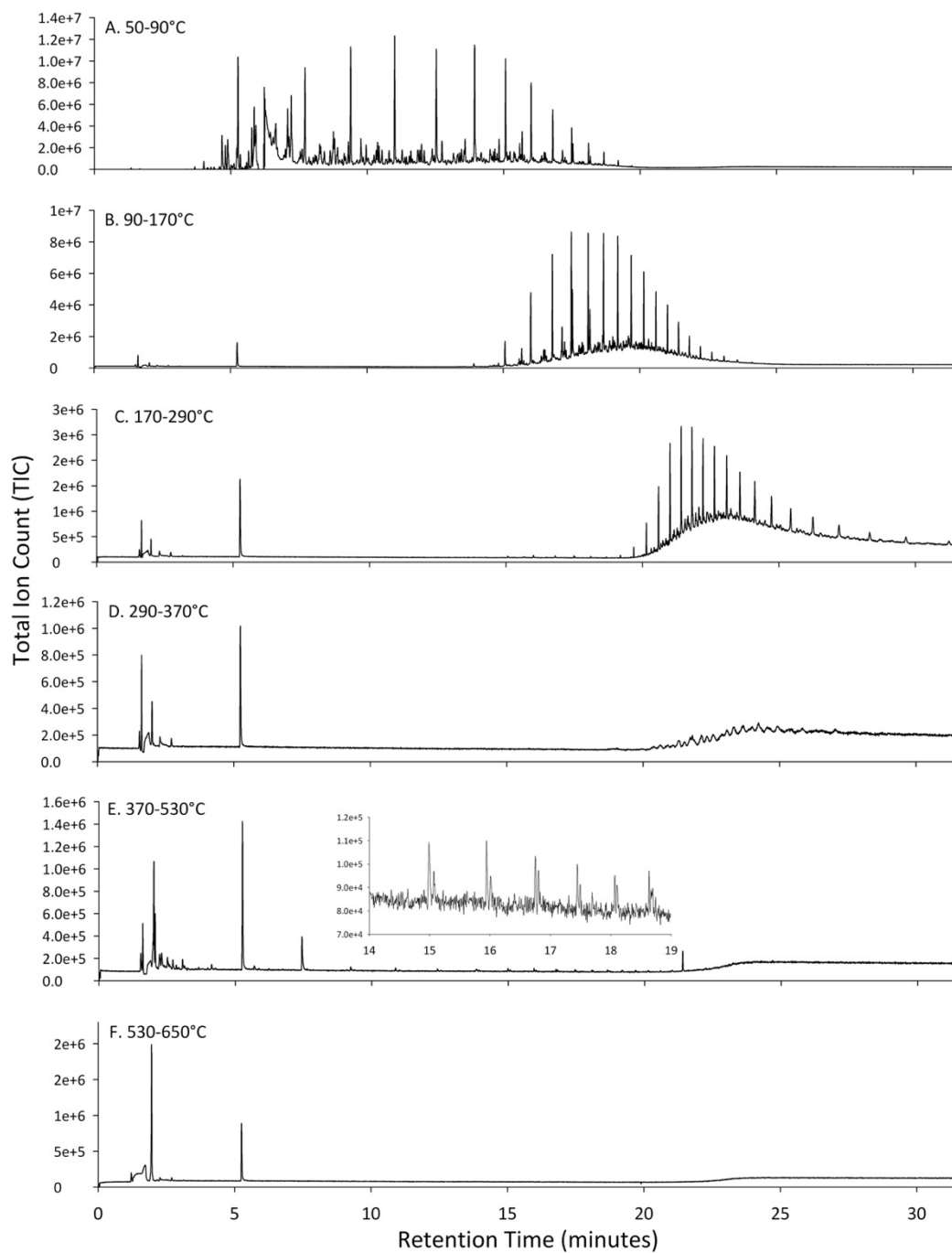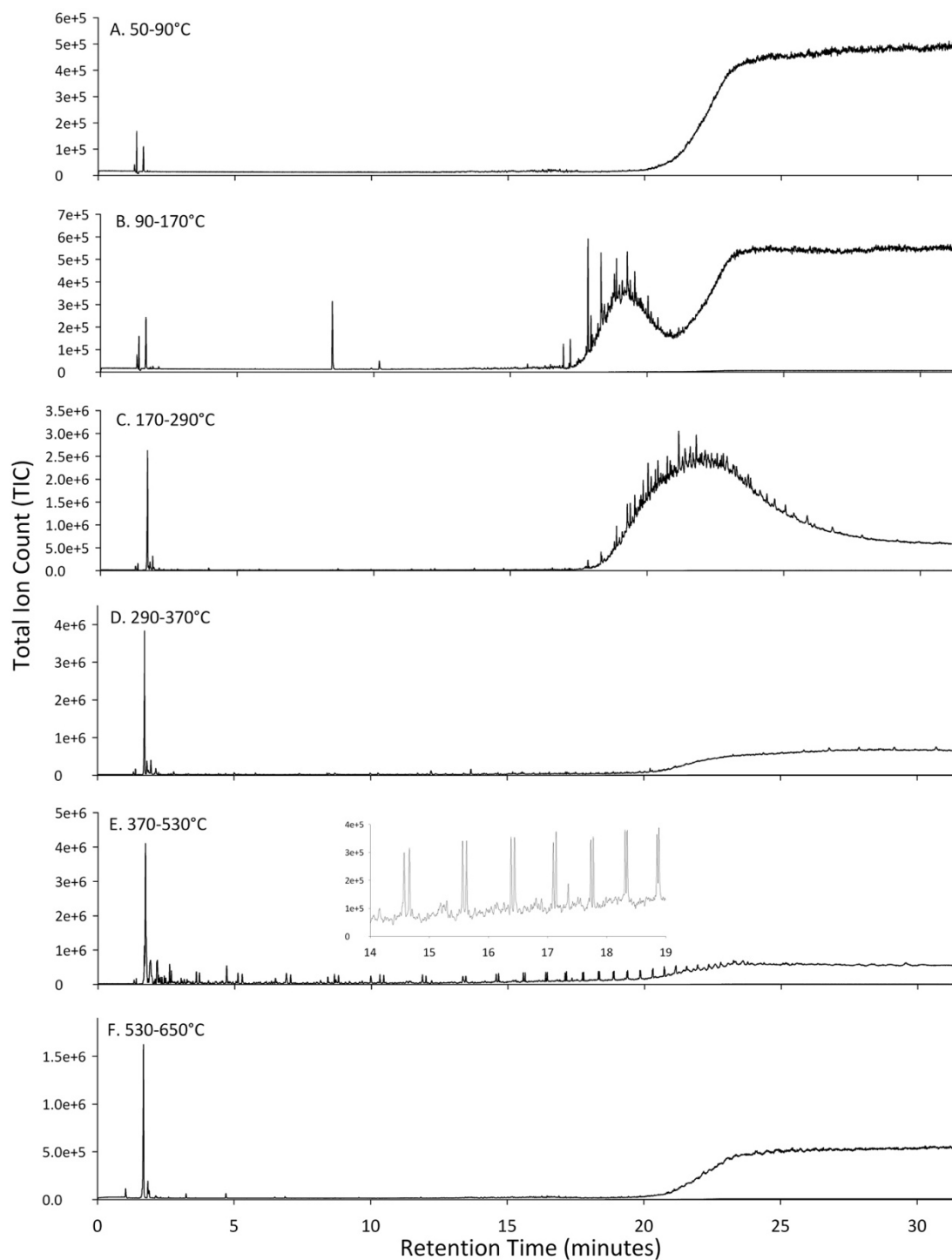**Figure 2.4** Six chromatograms are shown for each thermal slice of a 337 day tar sample, generated using thermal slicing Py-GC-MS. Note that the y-axis scale changes between slices, a result of varying content elution with temperature. The zoomed portion of Figure E is used to highlight the occurrence of thermal cracking.

59
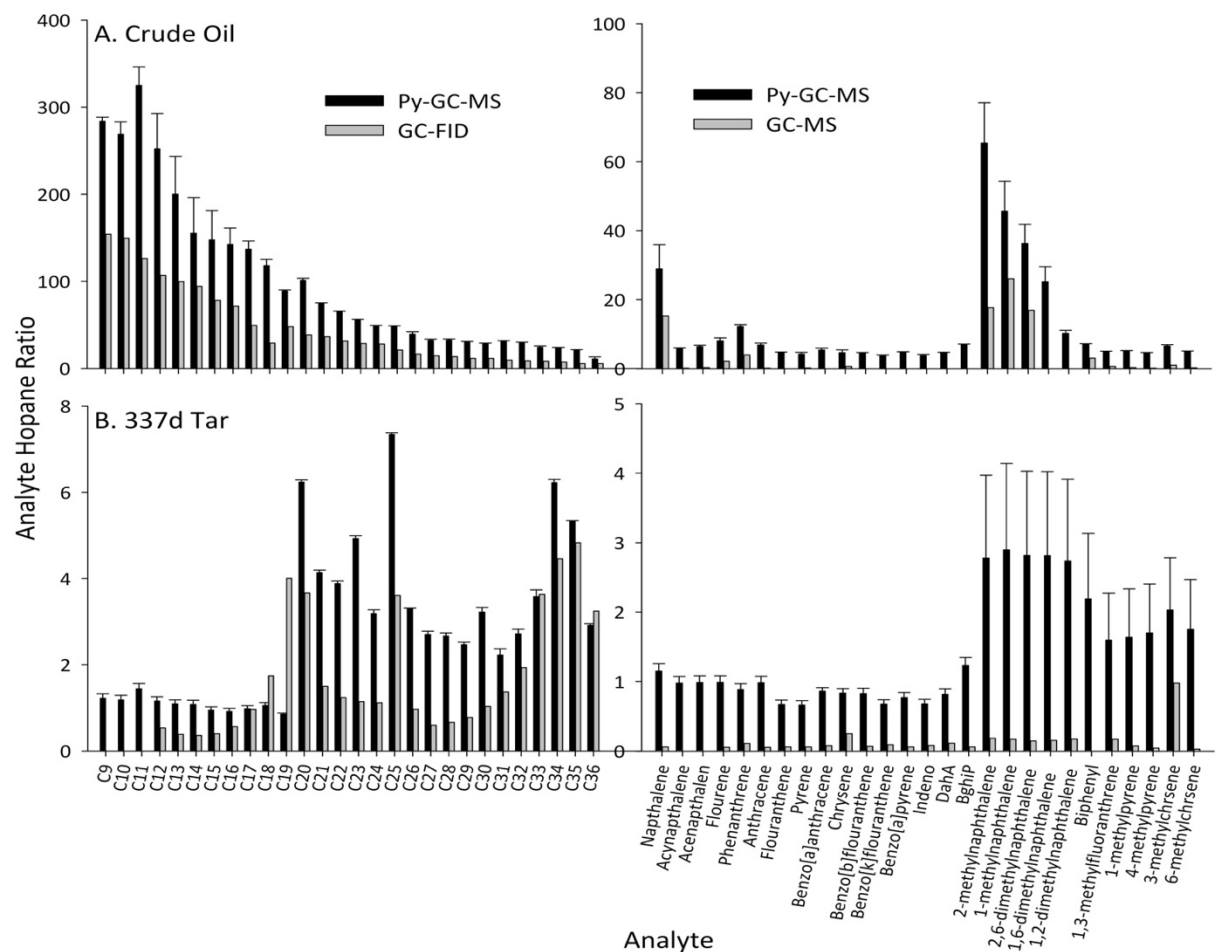
Figure 2.5 Compound concentrations normalized to C_{30}-hopane are shown for crude oil (A) and 337 d tar (B). Analyte concentration results from thermal slicing Py-GC-MS (black) are compared to results achieved by traditional chemical analysis (gray). Pyrolysis results are enriched in comparison. However, pyrolysis results follow similar concentration patterns, which are particularly illustrated by the *n*-alkane content.

60
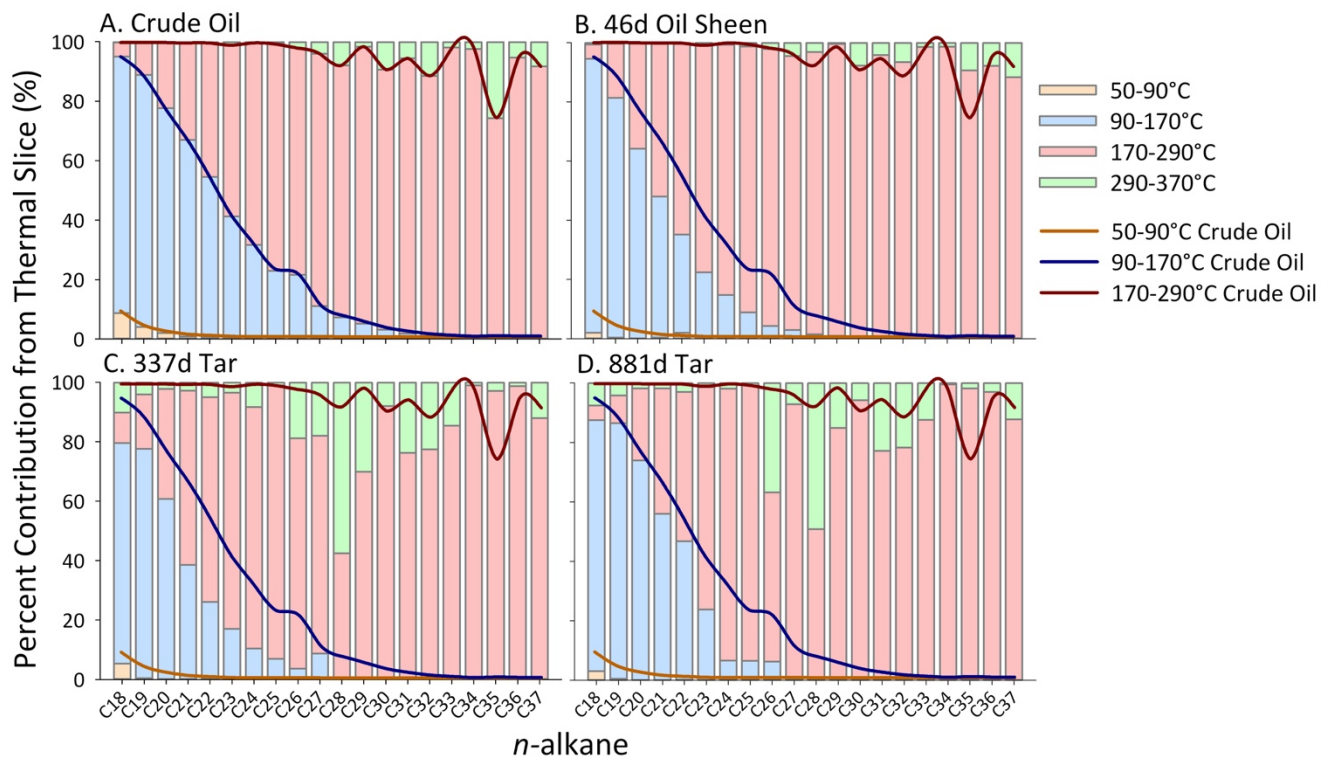
Figure 2.6 The percent of detected *n*-alkanes from each of the four quantification thermal slices is illustrated for four samples: A crude oil, B 46 d oil sheen, C 337 d tar and D 881 d tar. Percent contribution is determined based on the peak area of analyte normalized to the peak area of C_{30}-hopane. The curve for this distribution in crude oil is overlaid on each sample to illustrate how this changes between samples and thus, as a result of environmental weathering. More weathered samples require higher temperature for sublimation of *n*-alkanes, suggesting increased thermal stability with time. In particular, C_{26}-C_{33} alkane require high temperatures for sublimation from tar samples (C, D), as evidenced by significant elution in the 290-370°C slice.
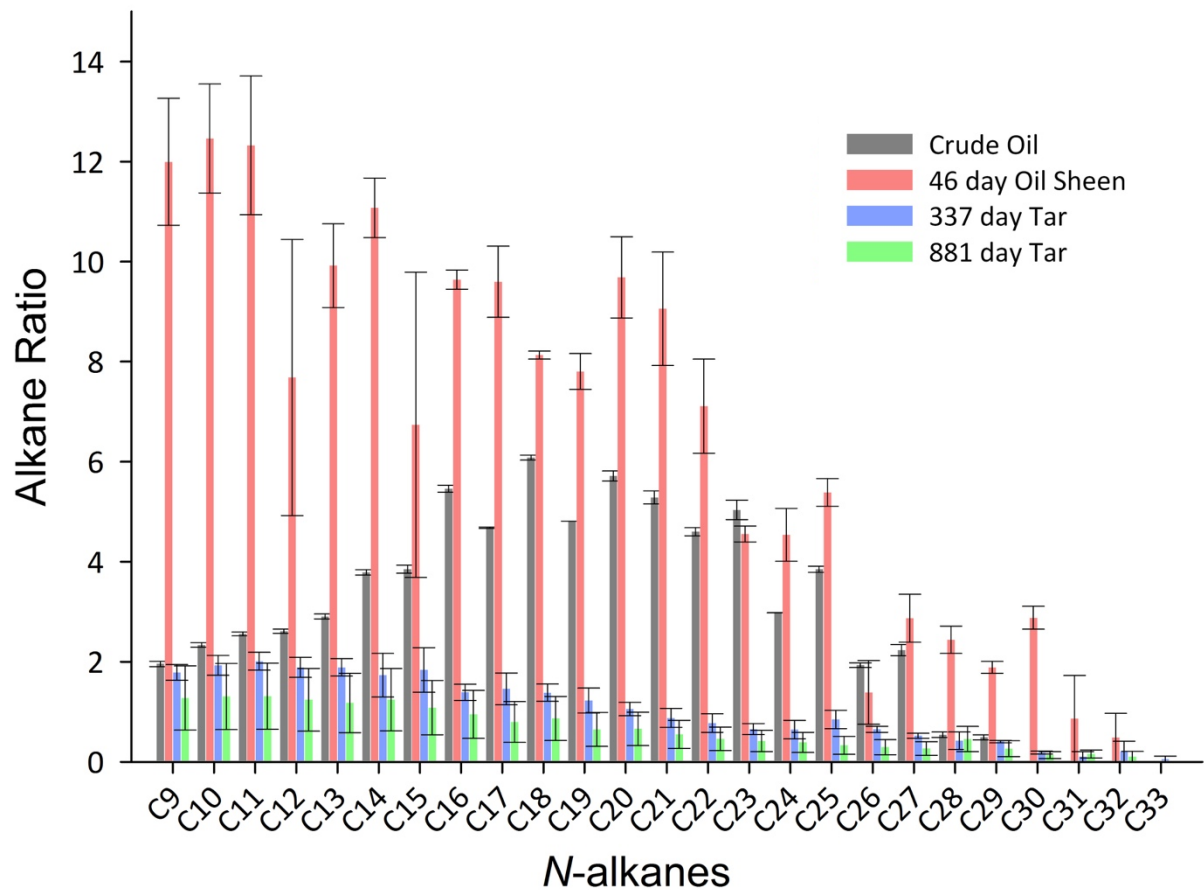
Figure 2.7 The amount of *n*-alkanes detected in thermal slices above 370°C are compared between crude oil, oil sheen and tar samples. *N*-alkane ratio is the alkane peak area normalized to sample weight and C_{30}-hopane peak area. Oil sheen has the highest alkane content for all alkanes (except C_{23} where it's slightly lower than crude oil), followed by crude oil. Tar samples and oil sheen have relatively similar alkane content <C_{13}, but tars and oil sheen have alkanes >C_{30}, while none were detected in crude oil. There was relatively little difference between the two tar samples.
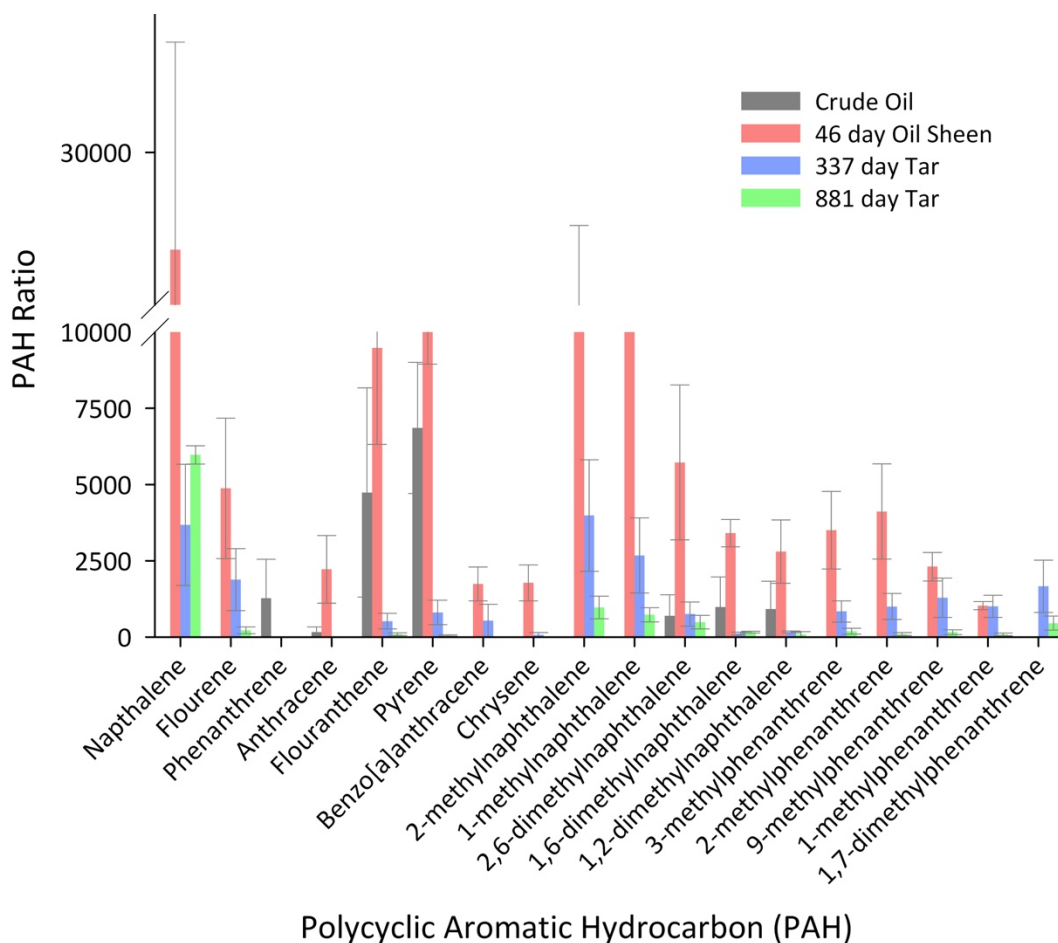
Figure 2.8 Detected PAHs and alkylated PAHs found in thermal slices above 370°C are compared between crude oil, oil sheen and tar samples. PAH ratio is the PAH peak area normalized to sample weight and C_{30}-hopane peak area. Relatively little PAH content was detected in the crude oil sample, and highest content was detected in 46 day oil sheen, followed by 337 day tar and 881 day tar samples.
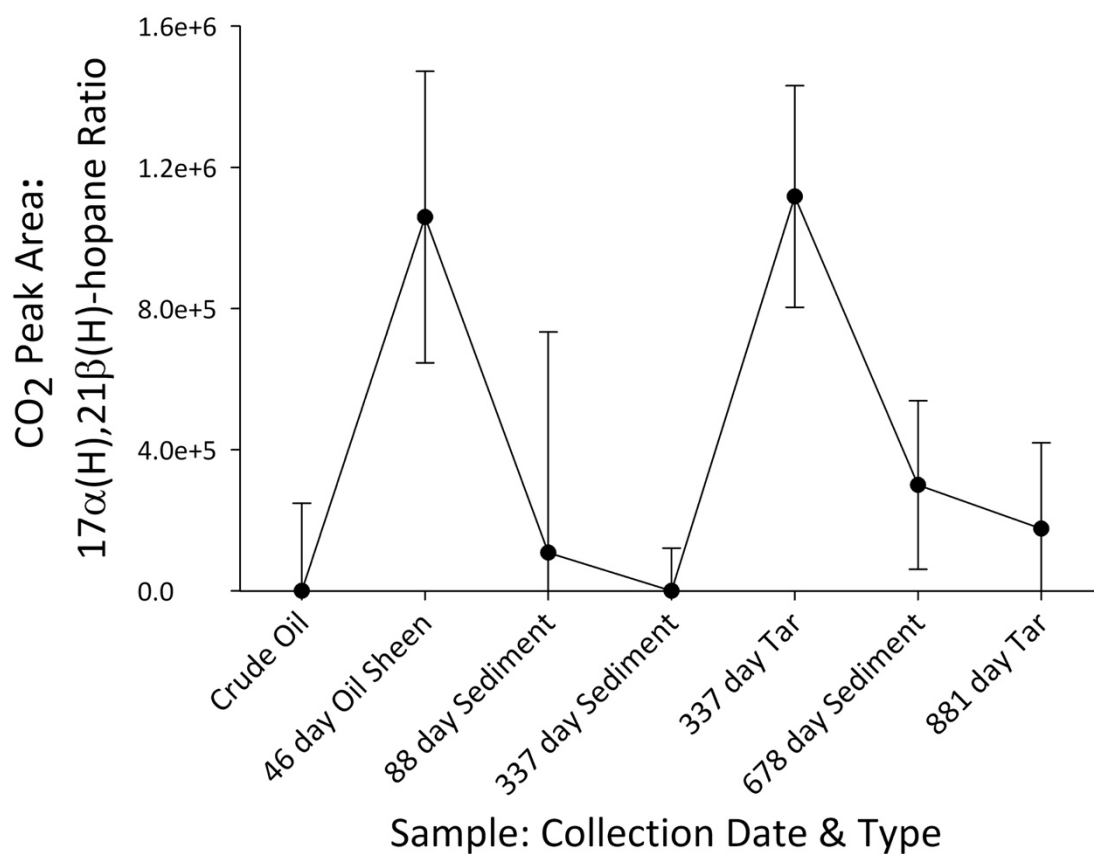
Figure 2.9 The sum of carbon dioxide peaks (CO_2) in all thermal slices, minus the CO_2 content found in blank runs and normalized to C_{30}-hopane is compared between seven samples. Highest content was found in the 46 d oil sheen, and second highest content in 337 d tar. Crude oil and 337 d sediment have zero CO_2 peaks. This can potentially be used to extrapolate oxygenated hydrocarbon content.

Conclusions

This study evaluates petroleum hydrocarbon weathering on a coastal Louisiana beach and salt marsh for three years following the *Deepwater Horizon* oil spill. This spill was the largest accidental oil spill ever reported and therefore, has been intensely studied in an attempt to elucidate marine hydrocarbon degradation patterns. Compared to previous research, we analyze compound specific degradation over time and across ecosystems, using both traditional and innovative analysis techniques.

Our results using traditional analysis techniques quantify GC amenable petroleum hydrocarbons and uniquely highlight how hydrogeography can enhance retention of toxic petroleum hydrocarbons in low energy environments. We believe this is a manifestation of wave energy in two ways: (1) directly, as low energy decreases physical advection of oil, thus decreasing dispersion, evaporation, and available dissolved oxygen and droplet surface area for biodegradation and (2) indirectly, as low energy sediments are fine-grained and have a larger sorption capacity for organic material, exacerbating environmental persistence. To our knowledge, this is the first study following the *Deepwater Horizon* spill to highlight the persistence of petroleum hydrocarbons, and compare this persistence across time and wave energy regimes. We believe this can inform policy makers and responders that the focus of remediation and prevention should be geared towards protecting low-energy marsh environments, as we report persistence of toxic hydrocarbons which could have many negative ramifications for species and ecosystem functionality.

Traditional analysis, however, is only suited to analyze GC amenable petroleum hydrocarbons, mainly a small fraction of saturates and aromatics. We employ ramped pyrolysis – gas chromatography – mass spectrometry (Py-GC-MS) as an alternative analysis technique. Using a bulk flow pyrolysis program, we look at the the elution patterns of organic material based on thermochemical stability, which we find correlates with total GC amenable hydrocarbon content. Therefore, bulk Py-GC-MS yields a rapid and holistic estimate of weathering in oiled samples, without tedious sample preparation and analysis.

We also analyze chromatograms created by thermal slicing Py-GC-MS, where analytes in a sample are separated by thermal energy of activation and analyzed via GC-MS. Chromatograms under 370°C contain traditionally GC amenable saturates and aromatics, which we quantify with an external standard curve. High temperature pyrolysis cracks non-traditionally GC amenable petroleum hydrocarbons (i.e. resins, asphaltenes and oxygenated hydrocarbons) into smaller compounds including n-alkanes, PAHs, alkylated PAHs and CO_2. We conclude that many of these compounds may be from the cracking of oxygenated species because of the high correlation between CO_2 and total alkanes and PAHs detected in this zone. Moreover, we speculate that these oxygenated parent hydrocarbons are (1) oxidized alkanes or oxidized alkane tails on larger hydrocarbons, which form alkanes/alkenes and CO_2 upon cracking, or (2) complex aromatic/resin/asphaltene in which the heteroatoms have been replaced with oxygen, which cracks into PAH and alkylated PAH species and CO_2. The oil sheen has the highest compound content in this high temperature zone, suggesting it is the most

66

oxidized. Moreover, tar samples have considerably more PAH cracking products than crude oil, suggesting that the complexity of asphaltene and resin conglomerations increases with the formation of tar.

Py-GC-MS has the ability to improve our understanding of oil weathering in the environment as part of the cadre of techniques typically use to analyze oil pollution, because it not only streamlines and simplifies traditional analysis, but also expands the analytical window to oxidized hydrocarbons, resins and asphaltenes. We suggest that this high temperature application is extremely useful, as oxidized hydrocarbons are difficult to quantify in samples. Although this cannot exactly detail parent structure, the quantification is sufficient to compare overall content between environmental samples. This also demonstrates the complexity of oil sheen, and the preservation of complex hydrocarbons in tar. Overall, this research should inform scientists, policy makers and pollution responders, alike, that complex hydrocarbons and toxic PAHs can persist in marsh coastal environments and that the research focus should shift to these ecosystems and the evaluation of complex oxygenated hydrocarbon species.

Appendix A

Table A.1 Analyte and quantifying ion used for analysis

Compound Name	m/z
n-alkanes	57
Naphthalene	128
Acenaphthylene	152
Acenapthelene	153
Fluorene	165
Phenanthrene	178
Anthracene	178
Fluoranthene	202
Pyrene	202
Benz[a]anthracene	228
Chrysene	228
Benzo[b]fluoranthene	252
Benzo[k]fluoranthene	252
Benzo[a]pyrene	252
Indeno[1,2,3-cd]pyrene	276
Dibenz[a,h]anthracene	278
Benzo[ghi]perylene	276
2-methylnaphthalene	142
1-methylnaphthalene	142
2,6-dimethylnaphthalene	156
2,3,5-trimethylnaphthalenne	155
1-methylfluorene	180
Dibenzothiophene	184
3-methylphenanthrene	192
2-methylphenanthrene	192
2-methylanthracene	192
9-methylphenanthrene	192
1-methylphenanthrene	192
4,6-dimethyldibenzothiophene	212
1,7-dimethylphenanthrene	206
3-methylfluoranthene	215
1-methylfluoranthene	216
Retene	219
1-methylpyrene	216
4-methypyrene	216
3-methylchrsene	242
6-methylchrsene	242
Benzo(e)pyrene	252

Table A.1 Continued

Perylene	252
αββ 20R-cholestane	217
ααα 20R-cholestane	217
αββ 20R 24S-methylcholestane	217
17α(H)-22,29,30-trisnorhopane	191
αββ 20R 24R-ethylcholestane	217
ααα 20R 24R-ethylcholestane	217
17α(H),21β(H)-30-norhopane	191
17α(H),21β(H)-hopane	191
17α(H),21β(H)-22S-homohopane	191
17α(H),21β(H)-22R-homohopane	191

Table A.2 Compound concentration in µg/mg sample. Samples organized by energy type and labeled based on collection date at Grand Isle. Sample denoted with * was collected in Bay Jimmy.

Analyte Type	Analyte Name	Oils		Tar Balls		Low Energy Sediments			High Energy Sediments		
		Crude	46	337	881	88	678	694*	88	337	678
Alkanes	C_{10} alkane	8647.34	0.00	0.00	0.00	0.00	0.00	0.00	0.00	0.00	0.00
	C_{11} alkane	8379.34	6.27	0.00	0.00	0.90	0.36	1.72	1.47	0.27	0.40
	C_{12} alkane	7079.16	63.33	14.64	14.60	0.84	0.56	7.65	1.56	3.78	1.48
	C_{13} alkane	6000.54	7.07	10.60	9.48	0.71	0.40	20.22	1.95	0.18	0.18
	C_{14} alkane	5587.09	22.03	9.93	9.59	0.82	0.92	72.61	3.76	0.19	0.17
	C_{15} alkane	5278.18	98.69	11.01	10.49	1.25	1.34	87.73	5.01	0.38	0.18
	C_{16} alkane	4387.82	322.80	15.46	13.34	2.06	1.19	57.33	9.79	0.99	0.26
	C_{17} alkane	4017.25	864.16	26.41	17.76	3.18	0.74	25.11	60.35	1.74	0.32
	C_{18} alkane	3374.54	1740.53	47.77	23.92	8.46	0.57	8.27	258.15	3.20	0.42
	C_{19} alkane	3471.83	2872.76	219.63	33.48	32.42	0.35	2.64	504.10	5.90	0.34
	C_{20} alkane	2685.75	3509.54	100.46	43.80	82.33	0.41	1.59	672.06	8.53	0.34
	C_{21} alkane	2164.42	2813.20	41.10	27.79	91.56	0.27	1.17	536.70	5.12	0.26
	C_{22} alkane	2049.56	2815.04	33.90	27.22	118.43	0.30	1.32	556.34	5.03	0.35
	C_{23} alkane	1766.09	2496.79	31.46	26.57	110.72	0.28	1.66	524.15	4.07	0.31
	C_{24} alkane	1611.00	2143.27	30.63	23.53	100.54	0.25	1.41	462.70	3.36	0.31
	C_{25} alkane	1577.55	1907.00	98.85	24.83	94.46	0.22	2.14	468.93	3.08	0.28
	C_{26} alkane	1186.62	1711.94	26.53	22.27	71.61	0.20	1.13	376.83	2.24	0.22
	C_{27} alkane	935.94	1403.00	16.34	19.49	58.19	0.19	2.95	306.19	1.44	0.25
	C_{28} alkane	814.46	1169.98	18.21	18.46	53.72	0.17	1.39	244.43	1.23	0.22
	C_{29} alkane	759.50	1080.76	21.27	20.55	48.72	0.20	5.37	226.32	1.07	0.22
	C_{30} alkane	655.58	885.44	28.37	22.27	37.41	0.17	1.39	187.65	1.09	0.20
	C_{31} alkane	644.74	868.43	37.64	23.28	39.66	0.18	4.89	175.13	1.16	0.19
	C_{32} alkane	533.81	657.16	52.96	26.26	29.83	0.17	1.18	130.59	1.15	0.15
	C_{33} alkane	479.69	589.22	99.68	31.75	27.52	0.17	2.74	111.56	1.73	0.22
	C_{34} alkane	462.01	496.70	122.28	38.05	23.59	0.16	0.90	89.38	2.07	0.16
	C_{35} alkane	415.00	404.15	132.44	37.81	19.68	0.14	1.20	65.94	1.98	0.19

Table A.2 Continued

	C_{36} alkane	320.59	259.60	88.86	28.11	14.88	0.14	0.69	47.91	1.18	0.17
	C_{37} alkane	310.35	309.11	113.64	34.80	16.89	0.17	0.83	53.57	1.45	0.20
	Σ[Alkanes]	75595.7	31518.0	1450.1	629.5	1090.4	10.2	317.2	6082.5	63.6	8.00
16 Priority EPA PAHs	Naphthalene	0.53	2.90	1.00	0.93	0.26	0.04	0.45	0.53	0.01	0.02
	Acenaphthylene	0.00	0.00	0.00	0.00	0.00	0.00	0.00	0.00	0.00	0.01
	Acenapthelene	0.42	2.09	0.00	0.00	0.20	0.05	1.70	0.42	0.00	0.01
	Fluorene	0.64	4.41	1.52	1.42	0.32	0.16	4.99	0.64	0.02	0.03
	Phenanthrene	1.09	22.42	3.06	2.80	0.55	0.20	7.18	1.09	0.08	0.04
	Anthracene	0.75	4.20	1.57	1.50	0.34	0.06	0.99	0.75	0.01	0.02
	Fluoranthene	0.61	3.81	1.68	1.49	0.28	0.04	0.25	0.61	0.01	0.02
	Pyrene	0.72	6.78	1.67	1.74	0.34	0.04	0.30	0.72	0.03	0.03
	Benz[a]anthracene	0.89	3.89	2.15	1.96	0.37	0.05	0.22	0.89	0.01	0.02
	Chrysene	2.30	14.28	6.88	4.05	1.03	0.08	0.25	2.30	0.06	0.07
	Benzo[b]fluoranthene	1.21	5.26	1.93	1.96	0.50	0.07	0.21	1.21	0.03	0.04
	Benzo[k]fluoranthene	1.15	3.39	2.49	2.38	0.40	0.07	0.24	1.15	0.02	0.02
	Benzo[a]pyrene	1.30	3.17	1.66	1.57	0.42	0.06	0.21	1.30	0.01	0.02
	Indeno[1,2,3-cd]pyrene	1.52	2.69	2.21	2.12	0.43	0.08	0.21	1.52	0.01	0.02
	Dibenz[a,h]anthracene	3.03	3.74	3.12	3.16	0.72	0.14	0.30	3.03	0.02	0.03
	Benzo[ghi]perylene	0.99	2.76	1.69	1.45	0.31	0.06	0.16	0.99	0.01	0.02
	Σ[16 Priority EPA PAHs]	17.15	85.80	32.64	28.53	6.46	1.20	17.64	17.15	0.34	0.42
Alkylated & Other PAHs	2-methylnaphthalene	146.33	3.73	5.02	4.77	0.35	0.08	4.57	0.73	0.04	0.06
	1-methylnaphthalene	99.37	3.13	4.67	4.36	0.29	0.12	2.45	0.62	0.03	0.05
	2,6-dimethylnaphthalene	9.43	3.65	4.04	3.83	0.35	0.08	18.05	0.74	0.03	0.04
	2,3,5-trimethylnaphthalenne	376.00	6.33	0.92	0.94	0.28	0.26	16.81	0.42	0.02	0.02
	1-methylfluorene	21.67	23.55	1.48	1.38	0.47	0.64	11.03	0.94	0.08	0.09
	Dibenzothiophene	9.91	5.59	1.44	1.32	0.16	0.51	2.35	0.38	0.02	0.05
	3-methylphenanthrene	20.50	53.74	4.23	3.98	0.78	0.08	3.38	2.08	0.15	0.06
	2-methylphenanthrene	20.40	72.44	4.87	4.59	0.98	0.17	4.90	2.73	0.20	0.06

71

Table A.2 Continued

	2-methylanthracene	3.56	4.20	2.86	2.84	0.39	0.20	1.78	0.82	0.02	0.03
	9-methylphenanthrene	23.17	67.25	3.96	3.74	0.77	0.08	2.04	2.56	0.17	0.05
	1-methylphenanthrene	17.02	56.43	3.93	3.62	0.86	0.12	2.27	2.37	0.17	0.06
	4,6-dimethyldibenzothiophene	94.93	36.52	1.63	1.52	0.43	0.13	0.53	1.18	0.09	0.12
	1,7-dimethylphenanthrene	90.17	48.02	3.18	3.08	1.04	0.08	0.50	2.35	0.20	0.05
	3 and 1 methylfluoranthene	6.47	18.60	4.66	5.83	0.93	0.11	0.42	1.54	0.09	0.11
	Retene	25.50	17.98	7.05	7.47	0.91	0.09	0.42	1.52	0.11	0.15
	1-methylpyrene	19.73	9.77	2.05	2.66	0.42	0.10	0.18	0.76	0.04	0.05
	4-methypyrene	9.03	5.21	1.24	1.70	0.30	0.04	0.19	0.59	0.02	0.02
	3-methylchrsene	58.27	16.54	26.81	15.41	0.76	0.04	0.25	1.43	0.45	0.43
	6-methylchrsene	15.73	11.49	0.76	1.54	0.69	0.07	0.23	1.14	0.06	0.07
	Benzo(e)pyrene	9.88	15.38	6.05	7.20	0.96	0.06	0.48	8.41	0.06	0.08
	Perylene	0.50	5.76	5.76	6.94	0.50	0.14	0.71	10.91	0.04	0.06
	Σ[Alkylated & Other PAHs]	1077.56	485.30	96.63	88.74	12.61	3.20	73.54	44.23	2.08	1.71
Hopanes and Steranes	αββ 20R-cholestane	40.23	131.15	42.04	12.92	5.68	0.29	0.74	24.86	1.08	0.46
	ααα 20R-cholestane	15.80	15.99	0.12	0.01	0.56	0.04	0.01	2.68	0.01	0.00
	αββ 20R 24S-methylcholestane	21.60	33.22	13.23	3.82	1.33	0.07	0.17	4.85	0.26	0.05
	17α(H)-22,29,30-trisnorhopane	13.03	17.48	5.95	2.56	1.01	0.05	0.14	3.29	0.16	0.08
	αββ 20R 24R-ethylcholestane	28.07	31.46	11.98	4.54	1.40	0.07	0.21	5.26	0.22	0.05
	ααα 20R 24R-ethylcholestane	15.90	25.34	29.58	11.22	1.10	0.05	0.14	5.20	0.78	0.17
	17α(H),21β(H)-30-norhopane	31.37	46.69	16.37	6.31	2.29	0.11	0.39	9.19	0.42	0.21
	17α(H),21β(H)-hopane	56.10	91.85	27.42	10.98	4.02	0.20	0.63	17.52	0.70	0.37
	17α(H),21β(H)-22S-homohopane	32.83	56.11	16.45	6.55	2.36	0.12	0.31	9.63	0.44	0.22
	17α(H),21β(H)-22R-homohopane	22.83	36.10	11.57	4.51	1.68	0.09	0.26	6.95	0.31	0.15
	Σ[Hopanes and Steranes]	277.77	485.38	174.71	63.42	21.45	1.09	3.01	89.43	4.38	1.76
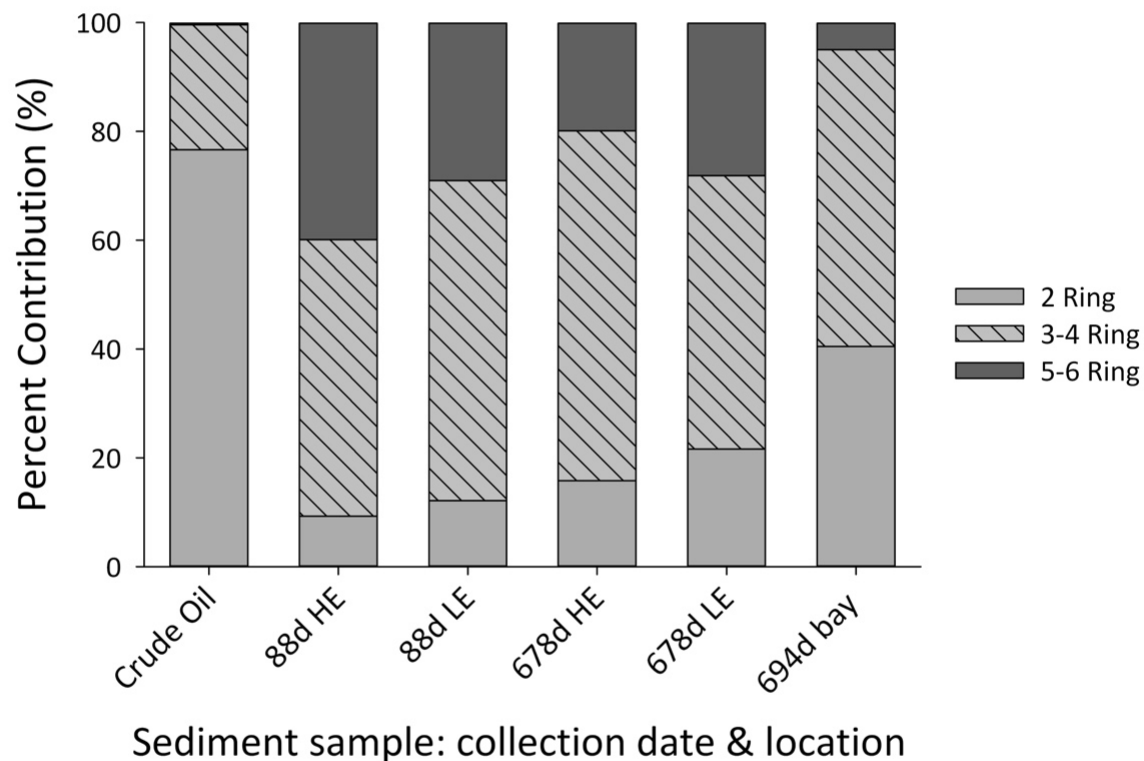
Figure A.1. PAHs in samples based on number of rings in PAHs. Samples labeled by collection date and energy type (HE = high energy and LE = low energy). 2-4 ring PAHs are preferentially weathered, so samples with higher percent of 2-4 ring PAHs are considered to be less weathered. This shows least weathering in crude oil, followed by bay sediment, low energy 678 d sediment, high energy 678 d sediment, low energy 88 d sediment and finally, high energy 88 d sediment.

Appendix B

Table B.1 Analytes and quantifying ions used for analysis.

Compound Name	m/z
n-alkanes	57
Naphthalene	128
Acenaphthylene	152
Acenapthelene	153
Fluorene	165
Phenanthrene	178
Anthracene	178
Fluoranthene	202
Pyrene	202
Benz[a]anthracene	228
Chrysene	228
Benzo[b]fluoranthene	252
Benzo[k]fluoranthene	252
Benzo[a]pyrene	252
Indeno[1,2,3-cd]pyrene	276
Dibenz[a,h]anthracene	278
Benzo[ghi]perylene	276
2-methylnaphthalene	142
1-methylnaphthalene	142
2,6-dimethylnaphthalene	156
2,3,5-trimethylnaphthalenne	156
3-methylphenanthrene	192
2-methylphenanthrene	192
2-methylanthracene	192
9-methylphenanthrene	192
1-methylphenanthrene	192
1,7-dimethylphenanthrene	206
Retene	234
1-methylpyrene	216
4-methypyrene	216
3-methylchrsene	242
6-methylchrsene	242
αββ 20R-cholestane	217
ααα 20R-cholestane	217
αββ 20R 24S-methylcholestane	217
17α(H)-22,29,30-trisnorhopane	191

Table B.1 Continued

αββ 20R 24R-ethylcholestane	217
ααα 20R 24R-ethylcholestane	217
17α(H),21β(H)-30-norhopane	191
17α(H),21β(H)-hopane	191
17α(H),21β(H)-22S-homohopane	191
17α(H),21β(H)-22R-homohopane	191

Table B.2 Summary of total contents from cracking zone, including the sum of CO_2, total alkanes and total PAHs. CO_2 was determined as the peak area (TIC), minus the peak area in blank run (TIC), normalized to C_{30}-hopane peak area (TIC) and sample weight. *N*-alkane and PAH ratio is the analyte peak area normalized to sample weight and C_{30}-hopane peak area, summed for all detected *n*-alkanes or PAHs and alkylated PAHs.

	CO_2	Total Alkane	Total PAH
Crude Oil	0.00	73.69	8,372.50
46 d Oil Sheen	1,058,991.00	160.53	56,251.33
87d Sediment	108,232.00	93.21	0.00
337 d Sediment	0.00	0.00	0.00
337 d Tar	1,117,615.00	25.92	36,145.00
678 d Sediment	289,792.33	78.80	0.14
881 d Tar	176,058.00	16.37	12810
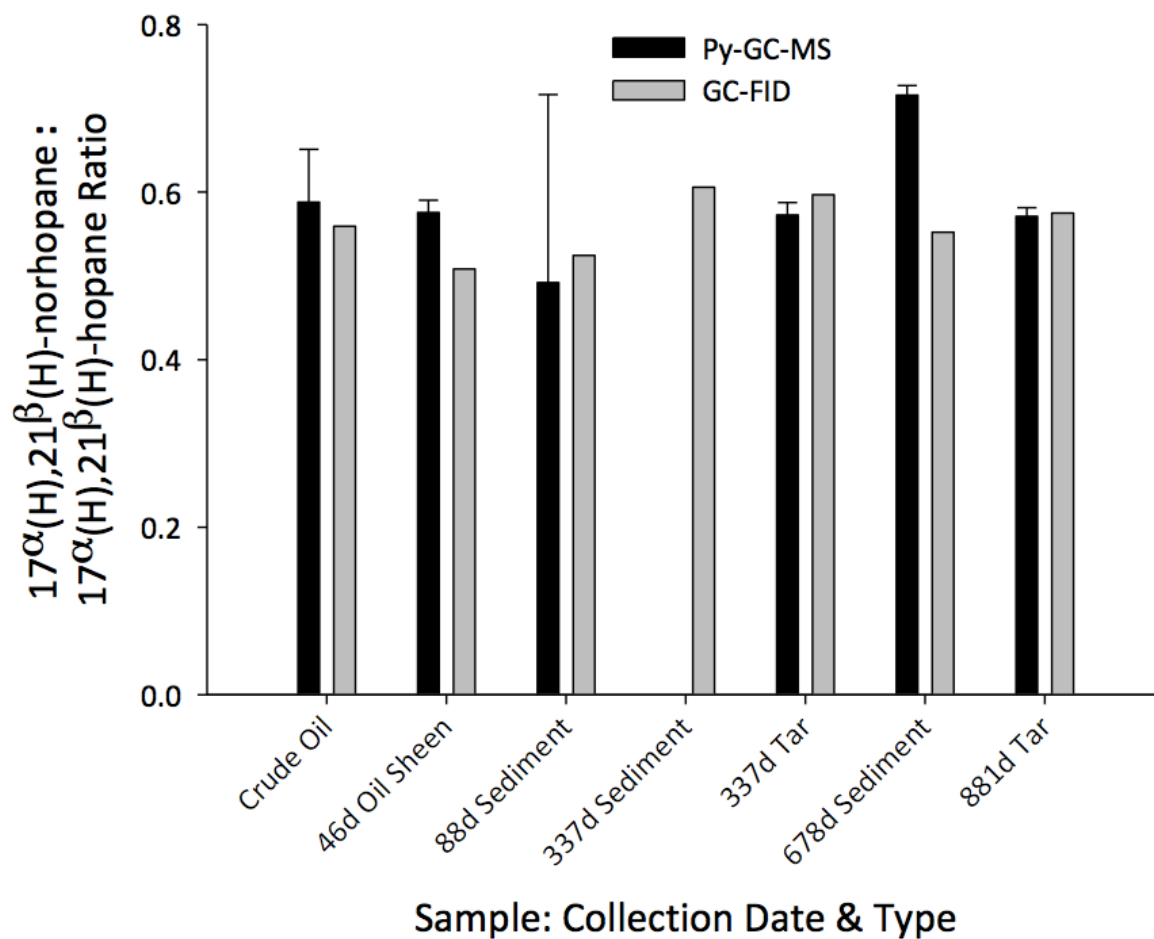
Figure B.1 Biomarker ratios for both traditional and Py-GC-MS methods, showing that all samples are from the *Deepwater Horizon* oil spill. For 337 d Sediment, no ratio is presented for Py-GC-MS because the $17\alpha(H),21\beta(H)$-norhopane sample peak was not large enough to reliably integrate.
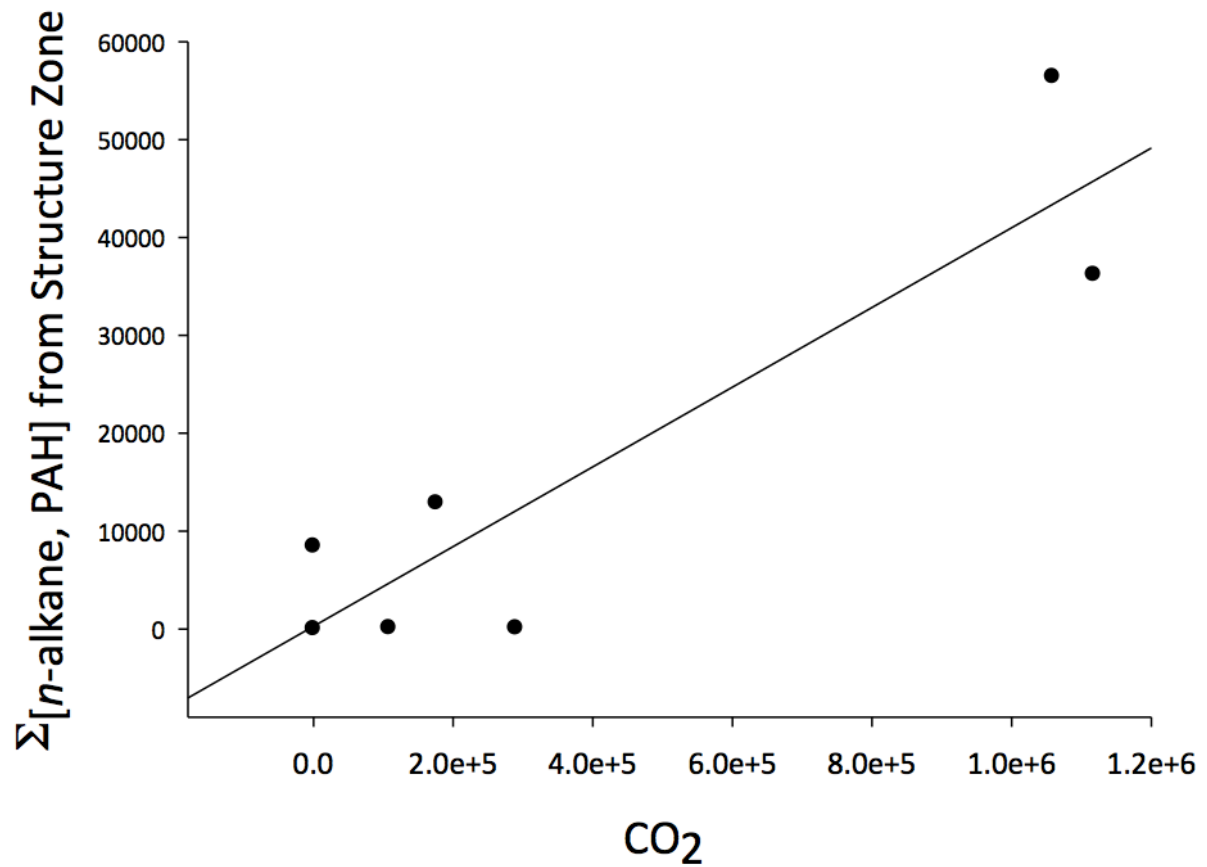
Figure B.2 Regression analysis comparing CO_2 from samples (Figure 2.9) with total n-alkane and PAH content from the structure zone (Figures 2.7 and 2.8). There's a positive linear correlation between the two values ($R^2 = 0.8179$), suggesting content within the structure zone may be related to CO_2 output.

References

1.   Michel, J. *et al*. Extent and Degree of Shoreline Oiling: Deepwater Horizon Oil Spill, Gulf of Mexico, USA. *PLoS One* **8,** 1–9 (2013).

2.   Reddy, C. M. *et al*. Composition and fate of gas and oil released to the water column during the Deepwater Horizon oil spill. *Proc. Natl. Acad. Sci. U. S. A.* **109,** 20229–34 (2012).

3.   McNutt, M. K. *et al*. Review of flow rate estimates of the Deepwater Horizon oil spill. *Proc. Natl. Acad. Sci.* **109,** 20260–20267 (2012).

4.   Lehr, B., Bristol, S. & Possolo, A. *Oil Budget Calculator Deepwater Horizon Technical Documentation*. (2010).

5.   Chanton, J. *et al*. Using Natural Abundance Radiocarbon To Trace the Flux of Petrocarbon to the Seafloor Following the Deepwater Horizon Oil Spill. *Environ. Sci. Technol.* (2014). doi:10.1021/es5046524

6.   Wang, Z. *et al*. Characteristics of spilled oils, fuels, and petroleum products: 1. Composition and properties of selected oils. *USEPA Publ.* **EPA/600/R-,** 1–286 (2003).

7.   Liu, Z., Liu, J., Zhu, Q. & Wu, W. The weathering of oil after the Deepwater Horizon oil spill: insights from the chemical composition of the oil from the sea surface, salt marshes and sediments. *Environ. Res. Lett.* **7,** 035302 (2012).

8.   Turner, R. E., Overton, E. B., Meyer, B. M., Miles, M. S. & Hooper-Bui, L. Changes in the concentration and relative abundance of alkanes and PAHs from the Deepwater Horizon oiling of coastal marshes. *Mar. Pollut. Bull.* **86,** 291–297 (2014).

9.   Camilli, R. *et al*. Tracking Hydrocarbon Plume Transport and Biodegradation at Deepwater Horizon. *Science (80-.).* **330,** 201–204 (2016).

10.   Stout, S. A., Payne, J. R., Emsbo-mattingly, S. D. & Baker, G. Weathering of field-collected floating and stranded Macondo oils during and shortly after the Deepwater Horizon oil spill. *Mar. Pollut. Bull.* (2016). doi:http://dx.doi.org/10.1016/j.marpolbul.2016.02.044

11. Bacosa, H. P., Erdner, D. L. & Liu, Z. Differentiating the roles of photooxidation and biodegradation in the weathering of Light Louisiana Sweet crude oil in surface water from the Deepwater Horizon site. *Mar. Pollut. Bull.* **95,** 265–272 (2015).

12. Sammarco, P. W. *et al.* Distribution and concentrations of petroleum hydrocarbons associated with the BP/Deepwater Horizon Oil Spill, Gulf of Mexico. *Mar. Pollut. Bull.* **73,** 129–43 (2013).

13. Lemelle, K. R., Elango, V. & Pardue, J. H. Distribution, characterization, and exposure of MC252 oil in the supratidal beach environment. *Environ. Toxicol. Chem.* **33,** 1544–51 (2014).

14. Urbano, M., Elango, V. & Pardue, J. H. Biogeochemical characterization of MC252 oil:sand aggregates on a coastal headland beach. *Mar. Pollut. Bull.* **77,** 183–91 (2013).

15. Kingston, P. F. Long-term environmental impact of oil spills. *Spill Sci. Technol. Bull.* **7,** 53–61 (2002).

16. Prince, R. C. *et al.* 17α(H),21β(H)-Hopane as a Conserved Internal Marker for Estimatlng the Biodegradation of Crude Oil. *Environ. Sci. Technol.* **28,** 142–145 (1994).

17. Wang, Z., Fingas, M. F. & Li, K. Fractionation of a Light Crude Oil and Identification and Quantitation of Alipatic, ARomatic and Biomarker Compounds by CG-FIDand GC-MS, Part I. *J. Chromatogr. Sci.* **32,** 361–366 (1994).

18. Aeppli, C. *et al.* Recalcitrance and degradation of petroleum biomarkers upon abiotic and biotic natural weathering of Deepwater Horizon oil. *Environ. Sci. Technol.* **48,** 6726–6734 (2014).

19. Lewan, M. D. *et al.* Asphaltene content and composition as a measure of Deepwater Horizon oil spill losses within the first 80days. *Org. Geochem.* **75,** 54–60 (2014).

20. Kiruri, L. W., Dellinger, B. & Lomnicki, S. Tar balls from deep water horizon oil spill: Environmentally persistent free radicals (EPFR) formation during crude weathering. *Environ. Sci. Technol.* **47,** 4220–4226 (2013).

21. Hall, G. J. *et al*. Oxygenated weathering products of Deepwater Horizon oil come from surprising precursors. *Mar. Pollut. Bull.* **75,** 140–149 (2013).

22. Aeppli, C. *et al*. Oil weathering after the Deepwater Horizon disaster led to the formation of oxygenated residues. *Environ. Sci. Technol.* **46,** 8799–807 (2012).

23. Aharon, P. Geology and biology of modern and ancient submarine hydrocarbon seeps and vents: An introduction. *Geo-Marine Lett.* **14,** 69–73 (1994).

24. Macdonald, I. R. *et al*. Natural oil slicks in the Gulf of Mexico visible from space. *J. Geophys. Res.* **98,** 16351 (1993).

25. Eckle, P., Burgherr, P. & Michaux, E. Risk of large oil spills: a statistical analysis in the aftermath of Deepwater Horizon. *Environ. Sci. Technol.* **46,** 13002–8 (2012).

26. Camilli, R. *et al*. Acoustic measurement of the Deepwater Horizon Macondo well flow rate. *Proc. Natl. Acad. Sci. U. S. A.* **109,** 20235–9 (2012).

27. BP Exploration & Production Inc. & Gulf of Mexico Alliance. *Gulf of Mexico Research Intiative Master Research Agreement*. (2015).

28. Wang, Z. & Fingas, M. F. Development of oil hydrocarbon fingerprinting and identification techniques. *Mar. Pollut. Bull.* **47,** 423–52 (2003).

29. Gutierrez, T. *et al*. Role of Bacterial Exopolysaccharides (EPS) in the Fate of the Oil Released during the Deepwater Horizon Oil Spill. *PLoS One* **8,** e67717 (2013).

30. Liu, Z. & Liu, J. Evaluating bacterial community structures in oil collected from the sea surface and sediment in the northern Gulf of Mexico after the Deepwater Horizon oil spill. *Microbiologyopen* **2,** 492–504 (2013).

31. Gros, J. *et al*. Resolving biodegradation patterns of persistent saturated hydrocarbons in weathered oil samples from the Deepwater Horizon disaster. *Environ. Sci. Technol.* **48,** 1628–1637 (2014).

32. King, G. M., Kostka, J. E., Hazen, T. C. & Sobecky, P. a. Microbial Responses to the Deepwater Horizon Oil Spill: From Coastal Wetlands to the Deep Sea. *Ann. Rev. Mar. Sci.* **7,** 377–401 (2015).

33. Cravo-Laureau, C. & Duran, R. Marine coastal sediments microbial hydrocarbon

degradation processes: contribution of experimental ecology in the omics'era. *Front. Microbiol.* **5,** 39 (2014).

34. Ruddy, B. M. *et al.* Targeted Petroleomics: Analytical Investigation of Macondo Well Oil Oxidation Products from Pensacola Beach. (2014).

35. Rashid, M. A. Degradation of Bunker C oil under different coastal environments of Chedabucto Bay, Nova Scotia. *Estuar. Coast. Mar. Sci.* **2,** 137–144 (1974).

36. Irvine, G. V., Mann, D. H. & Short, J. W. Multi-year persistence of oil mousse on high energy beaches distant from the Exxon Valdez spill origin. *Mar. Pollut. Bull.* **38,** 572–584 (1999).

37. Peterson, C. H. *et al.* Long-Term Ecosystem Response to the Exxon Valdez Oil Spill. **302,** 2082–2086 (2014).

38. Owens, E. H., Taylor, E. & Humphrey, B. The persistence and character of stranded oil on coarse-sediment beaches. *Mar. Pollut. Bull.* **56,** 14–26 (2008).

39. Pendergraft, M. a & Rosenheim, B. E. Varying relative degradation rates of oil in different forms and environments revealed by ramped pyrolysis. *Environ. Sci. Technol.* **48,** 10966–10974 (2014).

40. Wilson, M. J. *et al.* A Targeted Health Risk Assessment Following the Deep Water Horizon Oil Spill: Polycyclic Aromatic Hydrocarbon Exposure in Vietnamese-American Shrimp Consumers. *Environ. Health Perspect.* **152,** 152–159 (2014).

41. Lundstedt, S. *Analysis of PAHs and their transformation products in contaminated soil and remedial processes.* (2003).

42. Wang, Z. *et al.* Characterization and identification of the Detroit River mystery oil spill (2002). *J. Chromatogr. A* **1038,** 201–214 (2004).

43. Yin, F., John, G. F., Hayworth, J. S. & Clement, T. P. Long-term monitoring data to describe the fate of polycyclic aromatic hydrocarbons in Deepwater Horizon oil submerged off Alabama's beaches. *Sci. Total Environ.* **508,** 46–56 (2015).

44. Zengel, S., Bernik, B. M., Rutherford, N., Nixon, Z. & Michel, J. Heavily oiled salt marsh following the deepwater horizon oil spill, ecological comparisons of shoreline cleanup treatments and recovery. *PLoS One* **10,** 1–27 (2015).

45. Wang, Z. *et al*. Concentrations and sources of polycyclic aromatic hydrocarbons in surface coastal sediments of the northern Gulf of Mexico. *Geochem. Trans.* **15,** 1–12 (2014).

46. Kennish, M. J. *Ecology of Estuaries: Anthropogenic Effects*. (CRC Press, 1991).

47. Fathallah, S., Medhioub, M. N. & Kraiem, M. M. Photo-induced toxicity of four polycyclic aromatic hydrocarbons (PAHs) to embryos and larvae of the carpet shell clam Ruditapes decussatus. *Bull. Environ. Contam. Toxicol.* **88,** 1001–1008 (2012).

48. Denis, E. H. *et al*. Polycyclic aromatic hydrocarbons (PAHs) in lake sediments record historic fire events: Validation using HPLC-fluorescence detection. *Org. Geochem.* **45,** 7–17 (2012).

49. Yan, W., Chi, J., Wang, Z., Huang, W. & Zhang, G. Spatial and temporal distribution of polycyclic aromatic hydrocarbons (PAHs) in sediments from Daya Bay, South China. *Environ. Pollut.* **157,** 1823–1830 (2009).

50. Saha, M. *et al*. Sources of sedimentary PAHs in tropical Asian waters: Differentiation between pyrogenic and petrogenic sources by alkyl homolog abundance. *Mar. Pollut. Bull.* **58,** 189–200 (2009).

51. Zhang, S., Zhang, Q., Darisaw, S., Ehie, O. & Wang, G. Simultaneous quantification of polycyclic aromatic hydrocarbons (PAHs), polychlorinated biphenyls (PCBs), and pharmaceuticals and personal care products (PPCPs) in Mississippi river water, in New Orleans, Louisiana, USA. *Chemosphere* **66,** 1057–1069 (2007).

52. Venkatesan, M. I. Occurrence and possible sources of perylene in marine sediments-a review. *Mar. Chem.* **25,** 1–27 (1988).

53. Han, J. & Calvin, M. Hydrocarbon distribution of algae and bacteria, and microbiological activity in sediments. *Proc. Natl. Acad. Sci. U. S. A.* **64,** 436–443 (1969).

54. Blumer, M., Guillard, R. R. L. & Chase, T. Hydrocarbons of marine phytoplankton. *Mar. Biol.* **8,** 183–189 (1971).

55. Arulazhagan, P., Sivaraman, C., Kumar, S. A., Aslam, M. & Banu, J. R. Co-metabolic degradation of benzo(e)pyrene by halophilic bacterial consortium at different saline conditions. *J. Environ. Biol.* **35,** 445–452 (2014).

56. Rivas, F. J., Beltrán, F. J. & Acedo, B. Chemical and photochemical degradation of acenaphthylene. Intermediate identification. *J. Hazard. Mater.* **75,** 89–98 (2000).

57. Bence, A. E., Prince, R. C., Mcmillen, S. J. & Butler, E. L. Environmental Stability of Selected Petroleum Hydrocarbon Source and Weathering Ratios. **30,** 2332–2339 (1996).

58. Pendergraft, M. a *et al.* Linking ramped pyrolysis isotope data to oil content through PAH analysis. *Environ. Res. Lett.* **8,** 044038 (2013).

59. Sasser, C. E., Dozier, M. D., Gosselink, J. G. & Hill, J. M. Spatial and Temporal Changes in Louisiana Barataria Basin Marshes, 1945-1980. *Environ. Manage.* **10,** 671–680 (1986).

60. Fitzgerald, D. M., Kulp, M., Penland, S., Flocks, J. & Kindinger, J. Morphologic and stratigraphic evolution of muddy ebb-tidal deltas along a subsiding coast: Barataria Bay, Mississippi River delta. *Sedimentology* **51,** 1157–1178 (2004).

61. Chmura, G. L., Aharon, P., Socki, R. A. & Abernethy, R. An inventory of 13C abundances in coastal wetlands of Louisiana, USA: vegetation and sediments. *Oecologia* **74,** 264–271 (1987).

62. Silliman, B. R. *et al.* Degradation and resilience in Louisiana salt marshes after the BP - Deepwater Horizon oil spill. *Pnas* **109,** 11234–11239 (2012).

63. Shultz, J. M., Walsh, L., Garfin, D. R., Wilson, F. E. & Neria, Y. The 2010 Deepwater Horizon Oil Spill: The Trauma Signature of an Ecological Disaster. *J. Behav. Health Serv. Res.* 58–76 (2014). doi:10.1007/s11414-014-9398-7

64. Almeda, R. *et al.* Interactions between zooplankton and crude oil: toxic effects and bioaccumulation of polycyclic aromatic hydrocarbons. *PLoS One* **8,** e67212 (2013).

65. Valentine, D. L. *et al.* Fallout plume of submerged oil from   Deepwater

Horizon. *Proc. Natl. Acad. Sci.* **111,** 15906–15911 (2014).

66. Gopalan, B. & Katz, J. Turbulent shearing of crude oil mixed with dispersants generates long microthreads and microdroplets. *Phys. Rev. Lett.* **104,** 1–4 (2010).

67. McKenna, A. M. *et al.* Expansion of the Analytical Window for Oil Spill Characterization by Ultrahigh Resolution Mass Spectrometry: Beyond Gas Chromatography. *Environ. Sci. Technol.* **47,** 130619104044007 (2013).

68. Larter, S.R. Douglas, A. G. Pyrolysis methods in organic geochemistry: an overview. *J. Anal. Appl. Pyrolysis* **4,** 1–19 (1952).

69. Karacan, O. & Kok, M. V. Pyrolysis analysis of crude oils and their fractions. *Fuel Energy Abstr.* **38,** 391 (1997).

70. Tang, Y. C. & Stauffer, M. Development of multiple cold trap pyrolysis. *J. Anal. Appl. Pyrolysis* **28,** 167–174 (1994).

71. Tang, Y. & Stauffer, M. Multiple Cold Trap Pyrolysis Gas Chromatography: a new technique for modeling hydrocarbon generation. *Adv. Org. Chem.* **22,** 863–872 (1994).

72. Otto, S. *et al.* Pyrolysis–gas chromatography–mass spectrometry with electron-ionization or resonance-enhanced-multi-photon-ionization for characterization of polycyclic aromatic hydrocarbons in the Baltic Sea. *Anal. Chim. Acta* **885,** 60–69 (2015).

73. Otto, S. *et al.* Pyrolysis–gas chromatography–mass spectrometry with electron-ionization or resonance-enhanced-multi-photon-ionization for characterization of polycyclic aromatic hydrocarbons in the Baltic Sea. *Mar. Pollut. Bull.* **99,** 35–42 (2015).

74. Leinweber, P. & Schulten, H.-R. Advances in analytical pyrolysis of soil organic matter. *J. Anal. Appl. Pyrolysis* **49,** 359–383 (1999).

75. Rosenheim, Brad E., Santoro, Jenifer A., Gunter, Gunter, Domack, E. W. Improving antarctic sediment 14 c dating using ramped pyrolysis: an example from the hugo island trough. **55,** (2013).

76. Nuelle, M.-T., Dekiff, J. H., Remy, D. & Fries, E. A new analytical approach for

monitoring microplastics in marine sediments. *Environ. Pollut.* **184,** 161–9 (2014).

77.   Pendergraft, M. A. & Rosenheim, B. E. Varying relative degradation rates of oil in different forms and environments revealed by ramped pyrolysis. *Environ. Sci. Technol.* **48,** 10966–10974 (2014).

78.   Behar, F., Pelet, R. & Roucache, J. Geochemistry of asphaltenes. *Org. Geochem.* **6,** 587–595 (1984).

79.   Groenzin, H. & Mullins, O. C. Asphaltene Molecular Size and Structure. *J. Phys. Chem. A* **103,** 11237–11245 (1999).

80.   Groenzin, H. & Mullins, O. C. Molecular Size and Structure of Asphaltenes from Various Sources. *Energy & Fuels* **14,** 677–684 (2000).

81.   Keiluweit, M., Kleber, M., Sparrow, M. a., Simoneit, B. R. T. & Prahl, F. G. Solvent-extractable polycyclic aromatic hydrocarbons in biochar: Influence of pyrolysis temperature and feedstock. *Environ. Sci. Technol.* **46,** 9333–9341 (2012).

82.   Antal, M. J. & Grønli, M. The Art, Science, and Technology of Charcoal Production. *Ind. Eng. Chem. Res.* **42,** 1619–1640 (2003).

83.   Mclean, J. D. & Kilpatrick, P. K. Effects of Asphaltene Solvency on Stability of Water-in-Crude-Oil Emulsions. *J. Colloid Interface Sci.* **189,** 242–253 (1997).

84.   Leontaritis, J. Asphaltene Deposition : A Comprehensive Description of Problem Manifestations and Modeling Approaches. *Soc. Pet. Eng. J.* **18892,** 15 (1989).

85.   Carbognani, L., Lubkowitz, J., Gonzalez, M. F. & Pereira-Almao, P. High temperature simulated distillation of Athabasca vacuum residue fractions. Bimodal distributions and evidence for secondary 'on-column' cracking of heavy hydrocarbons. *Energy and Fuels* **21,** 2831–2839 (2007).

86.   Asaoka, S. & Nakata, S. Asphaltene cracking in catalytic hydrotreating of heavy oils. 2. Study of changes in asphaltene structure during catalytic hydroprocessing. *Ind. Eng. …* 242–248 (1983). doi:10.1021/i200021a013

87.   Sahimi, M., Rassamdana, H. & Dabir, B. Asphalt formation and precipitation: Experimental studies and theoretical modelling. *SPE J.* **2,** 157–169 (1997).

88.   Rassamdana, H., Dabir, B., Nematy, M., Farhani, M. & Sahimi, M. Asphalt

flocculation and deposition: I. The onset of precipitation. *{AIChE} J.* **42,** 10–22 (1996).

89. Warnock, A. M., Hagen, S. C. & Passeri, D. L. Marine tar residues: A review. *Water. Air. Soil Pollut.* **226,** 66– (2015).

90. Hammami, A. & Raines, M. A. Paraffin Deposition From Crude Oils: Comparison of Laboratory Results With Field Data. *SPE J.* **4,** 9–18 (1999).

91. Hansen, J. H., Fredenslund, A., Pedersen, K. S. & Røningsen, H. P. A Thermodynamic Model for Predicting Wax Formation in Crude Oils. *AIChE J.* **34,** 1937–1942 (1988).

92. Peng, X. *et al.* Optimization of ultrasonic extraction and clean-up protocol for the determination of polycyclic aromatic hydrocarbons in marine sediments by high-performance liquid chromatography coupled with fluorescence detection. *J. Ocean Univ. China* **11,** 331–338 (2012).

93. Berset, J. D., Ejem, M., Holzer, R. & Lischer, P. Comparison of different drying, extraction and detection techniques for the determination of priority polycyclic aromatic hydrocarbons in background contaminated soil samples. *Anal. Chim. Acta* **383,** 263–275 (1999).

94. Filipkowska, A., Lubecki, L. & Kowalewska, G. Polycyclic aromatic hydrocarbon analysis in different matrices of the marine environment. *Anal. Chim. Acta* **547,** 243–254 (2005).

95. O'Connell, S. G., Haigh, T., Wilson, G. & Anderson, K. a. An analytical investigation of 24 oxygenated-PAHs (OPAHs) using liquid and gas chromatography-mass spectrometry. *Anal. Bioanal. Chem.* **405,** 8885–96 (2013).

96. Ong, R., Lundstedt, S., Haglund, P. & Marriott, P. Pressurised liquid extraction-comprehensive two-dimensional gas chromatography for fast-screening of polycyclic aromatic hydrocarbons in soil. *J. Chromatogr. A* **1019,** 221–232 (2003).

97. Nassar, N. N., Hassan, A. & Pereira-Almao, P. Application of nanotechnology for heavy oil upgrading: Catalytic steam gasification/cracking of asphaltenes. *Energy and Fuels* **25,** 1566–1570 (2011).

98.   Speight, J. G. High Temperature Mass Spectroscopy of Athabasca Asphaltenes and the Relationship To Cracking Processes.

99.   Williams, E. K., Rosenheim, B. E., McNichol, A. P. & Masiello, C. A. Charring and non-additive chemical reactions during ramped pyrolysis: applications to the characterization of sedimentary and soil organic material. *Org. Geochem.* **77,** 106–114 (2014).

100. Burns, K. a. Evidence for the importance of including hydrocarbon oxidation products in environmental assessment studies. *Mar. Pollut. Bull.* **26,** 77–85 (1993).

101. Ukiwe, L. N., Egereonu, U. U., Njoku, P. C., Nwoko, C. I. a. & Allinor, J. I. Polycyclic Aromatic Hydrocarbons Degradation Techniques: A Review. *Int. J. Chem.* **5,** 43–55 (2013).

102. Faksness, L.-G., Altin, D., Nordtug, T., Daling, P. S. & Hansen, B. H. Chemical comparison and acute toxicity of water accommodated fraction (WAF) of source and field collected Macondo oils from the Deepwater Horizon spill. *Mar. Pollut. Bull.* **91,** 222–229 (2014).

103. Carmichael, C. A. *et al.* Floating oil-covered debris from Deepwater Horizon: identification and application. *Environ. Res. Lett.* **7,** 15301 (2012).

104. Kokaly, R. F. *et al.* Spectroscopic remote sensing of the distribution and persistence of oil from the Deepwater Horizon spill in Barataria Bay marshes. *Remote Sens. Environ.* **129,** 210–230 (2013).

Vita

Meredith Moss Evans is from Dallas, TX, but spent a large part of her life in Aurora, IL. After graduating from Flower Mound High School in Flower Mound, TX she completed her B.S. magna cum laude in Biology with a minor in Spanish Language at the University of Oklahoma. She plans to continue merging her love of the ocean and passion for pollution science in her further career.

Permanent email: m.evans@utexas.edu